Mechanism of the Passivation of Zirconium in Low pH Solutions

James Arthur VanWinkle

B.S. Physics, Oregon State University, 1987

M.S. Nuclear Engineering, Oregon State University, 1989

M.S. Environmental Science and Engineering, Oregon Graduate Institute of Science and Technology, 1996

A dissertation presented to the faculty of the

Oregon Graduate Institute of Science and Technology

in partial fulfillment of the

requirements for the degree

Ph.D.

in

Materials Science and Engineering

January, 1999

The dissertation "Mechanism of the Passivation of Zirconium in Low pH Solutions" by James VanWinkle has been examined and approved by the following Examination Committee:

Dr. Margaret Ziomek-Moroz, Thesis Advisor
Associate Professor
Department of Materials Science and Engineering
Oregon Graduate Institute of Science and Technology

Dr. David Atteridge, Professor
Department of Materials Science and Engineering
Oregon Graduate Institute of Science and Technology

Dr. Jack McCarthy, Assistant Professor
Department of Materials Science and Engineering
Oregon Graduate Institute of Science and Technology

Dr. Te-Lin Yau, Metallurgist and Corrosion Engineer
Te-Lin Yau Consultancy
Albany, Oregon

Acknowledgements

I would like to thank Oremet-Wah Chang, Albany for supporting this research. I would specifically like to thank Derrill Holmes, Jack Tosdale, Jeff Fahey,John Haygarth and Te-Lin Yau and for their help. I would also like to thank the Department of Energy, Albany Research Center for the use of their XPS equipment. Specifically, I would like to thank Bernie Covino and Sophie Bullard of DOE for their help. I'd like to thank my committee for their time and advice. I would also like to thank Wei Su, formerly of OGI, for all of his help, support and advice. And finally, I would like to thank Margaret Ziomek-Moroz of OGI for her tireless support, patience and effort in helping complete this Opus.

Dedication

Love ya, Ma.

Table of Contents

List of Tables

List of Figures

Abstract

Mechanism of the Passivation of Zirconium in Low pH Solutions

James VanWinkle

Supervising Professor, Dr. Margaret Ziomek-Moroz

The passivation of zirconium alloys Zr-702 and Zr-704 was investigated using electrochemical and surface analysis techniques. The techniques used in this research include electrochemical experiments, such as potentiodynamic, potentiostatic, and electrochemical impedance spectroscopy (EIS), optical and scanning electron microscopy (SEM), energy dispersive x-ray spectroscopy (EDS), and x-ray photoelectron spectroscopy (XPS),.

The electrochemical experiments results showed that both alloys passivated in sulfuric acid. This passivity was modified by reducing the water content of the solution by adding methanol to the electrolyte. Both alloys showed transpassive behavior in hydrochloric acid and aqueous-methanolic sulfuric acid. Microscopic analysis of samples after the potentiostatic experiments in hydrochloric acid showed pitting. Potentiostatic measurements showed that both alloys remain passive in hydrochloric acid.

SEM/EDS and XPS chemical analyses showed that the passive film consisted of only zirconium and oxygen. The XPS results showed that the zirconium in the film was in either the 0 or +4 state. Additionally, XPS showed that the thickest films were formed in aqueous sulfuric acid. Films formed in hydrochloric acid showed no thickness increase over air-formed films.

EIS analyses showed that the passive films formed on both alloys in sulfuric and hydrochloric acid grow under diffusion control. Mott-Schottky EIS analyses showed that the passive films formed were semiconductor in nature, and had donor densities on the order of 10^{19} cm^{-3}.

1.0 Introduction

Zirconium alloys were originally developed as structural materials for the nuclear industry because of their low thermal neutron cross-section and good corrosion resistance in hot water. [1] Although the traditional use of zirconium has been in the cladding of nuclear fuel rods, it is gaining popularity as a corrosion-resistant material in the chemical industry, replacing alloys such as stainless steel. Zirconium is very active chemically, but it exhibits excellent corrosion resistance in most oxidizing and non-oxidizing media due to the formation of an adherent passive film.[2] This phenomenon is well known; however, the mechanism behind the formation of the passive film in these media is not well understood and must be investigated in order to develop or modify existing technological processes, such as chemical cleaning. [3]

Zirconium products are manufactured in a wide variety of shapes and sizes, including plates, sheets, rods, wires and tubes. These components are used for constructing highly corrosion-resistant equipment, such as heat exchangers, condensers, columns, reactors, piping systems, tanks, pumps and valves, as well as the more traditional fuel rod cladding used in the nuclear industry.[1,2]

The manufacturing process for zirconium products involves machining, forming, cleaning and welding. The cleaning processes include chemical cleaning, mechanical cleaning, pickling (acid cleaning/treatment), and descaling.[3] Some applications of zirconium products require a smooth surface finish. This surface smoothing is accomplished by mechanical honing and/or sandblasting, followed by an acid cleaning to remove surface contamination and to smooth the surface. The acid cleaning process uses an aqueous mixture of nitric and hydrofluoric acids, with a 10:1 ratio of nitric to hydrofluoric acids.[2] Although the surface quality of products prepared this way is very high, there exists a need to replace them with a single process which will replace the hydrofluoric/nitric pickle, allow recovery of zirconium ions from the cleaning process for

recycle, and produce an equivalently clean surface.[3] One possible replacement for the chemical cleaning would be an electrochemical process.[3]

To develop an economical electrochemical process to meet the goals outlined above, it is necessary to study the corrosion behavior of zirconium and its alloys in suitable electrolytes. The electrochemical process must not lead to localized corrosion, but rather must form and break down a passive surface film uniformly across the surface. To develop a process in which this surface film forms and breaks down uniformly, it is vital to understand the mechanism of film formation. The goal of this research is to determine the mechanism of passive film formation of zirconium in aqueous and aqueous-alcoholic electrolytes.

2.0 Literature Review

2.1 Zirconium and Zirconium Alloys

2.1.1 Physical Properties of Zirconium and Zirconium Alloys

Zirconium (Atomic Number 40) is a grey-white ductile metal, first developed for use in nuclear reactors due to its low thermal neutron cross-section. [1] It is a reactive metal ($E_o = -1.57V_{SHE}$), with a strong affinity for oxygen. [2] Because of this affinity, zirconium forms a tightly adherent oxide film (ZrO_2) in media containing oxygen. This film is the reason for the excellent corrosion behavior of zirconium in both oxidizing and reducing solutions. [2]

Zirconium has a hexagonal crystal structure at room temperature, with a transition to a body centered cubic lattice at 865°C. The hcp structure gives zirconium anisotropic physical and mechanical properties. [1]

2.1.2 Zirconium Alloys

Zirconium alloys come in two general types: nuclear and non-nuclear.[1,2] In the nuclear alloys, the naturally occurring hafnium present in zirconium ores is removed.[1] Hafnium has little effect on the mechanical and chemical properties of zirconium alloys, but has a dramatic impact on the nuclear properties because of its high thermal neutron cross-section.[2] Common alloying elements added to zirconium include niobium, iron, chromium, nickel and tin. [1,2] A list of nuclear-grade zirconium alloys is shown in Table 2-1. [2] Nuclear-grade alloys are used as fuel rod cladding, flow channels, guide tubes, spacer grids, and nuclear fuel rod end plugs. [2]

Table 2-1. Chemical Composition of Nuclear Grade Zirconium Alloys

Alloy	Zr+ Hf min	Hf max	Sn	Nb	Fe	Cr	Ni	Fe+Cr	Fe+Cr +Ni	O max
Zircaloy-2	–	0.01	1. 2- 1.7	–	0.07- 0.20	0.05- 0.15	.03- .08	–	0.18- 0.38	--
Zircaloy-4	--	0.01	1. 2- 1.7	--	0.18- 0.24	0.07- 0.13	–	0.28- 0.37	–	--
Zr-2.5Nb	--	0.01	--	2.4- 2.8	–	–	–	–	–	--

Non-nuclear zirconium alloys are used in many forms, including tubes, heat exchangers, piping, evaporators, tanks, valves and packings used in the chemical process industry. [2] A list of non-nuclear grade zirconium alloys is given in Table 2-2

Table 2-2. Chemical Composition of Non-Nuclear Zirconium Alloys

Alloy name	Zr+ Hf min	Hf max	Sn	Nb	Fe	Cr	Ni	Fe+Cr	Fe+ Cr+ Ni	O max
Zr-702	99.2	4.5	–	–	–	–	--	0.2 max	--	0.16
Zr-704	97.5	4.5	1.0-2.0	–	--	--	--	0.2-0.4	--	0.18
Zr-705	95.5	4.5	--	2.0-3.0	–	–	--	0.2 max	--	0.18
Zr-706	95.5	4.5	--	2.0-3.0	–	–	--	0.2 max	–	0.16

In this research, the non-nuclear zirconium alloys, Zr-702 and Zr-704 were studied. Zr-702 is unalloyed zirconium, and was chosen to give a baseline of data for zirconium behavior.[1] ZR-704 is the non-nuclear analog to the alloy Zircaloy-4, and is used in a number of applications.[2] ZR-704 differs from ZR-702 in that it has small amounts of tin, iron, and chromium added.

2.1.3 Corrosion Behavior of Zirconium

2.1.3.1 Dissolution

Zirconium and ZrO_2 dissolve in hydrofluoric acid (HF) and hot, concentrated sulfuric acids [4], aqua regia, and mixtures of HCl and HNO_3 [2] . In hydrofluoric acid, the relevant reactions are:

$$Zr + 4HF \longrightarrow ZrF_4 + 2H_2 \quad (2\text{-}1)$$

$$ZrO_2 + 4HF \longrightarrow ZrF_4 + 2H_2O \quad (2\text{-}2)$$

$$ZrF_4 + 2HF \longrightarrow H_2ZrF_6 \longrightarrow 2H^+ + ZrF_6^{2-} \quad (2\text{-}3)$$

At high temperatures and concentrations, zirconium corrodes in sulfuric acid because the surface film formed is not ZrO_2, but zirconium disulfate tetrahydrate $[Zr(SO_4)_2 \cdot 4H_2O]$. [2] At very high sulfuric acid concentrations, the film that flakes off also contains zirconium hydrides. [2]

2.1.3.2 Passivation

Passive films on metals provide a thin, protective layer which acts as a barrier to further reaction. [5] These layers can be formed by chemical or mechanical passivation. Chemical passivation involves forming a chemical compound on the surface of the material by chemical or electrochemical action. Mechanical passivation occurs when ions dissolved from a surface precipitate onto that surface. The passivation of zirconium is associated with the formation of a thin oxide layer, but the mechanism of the formation of this passive layer is still unknown.[2] Studies have shown that the potential at which the film is formed has an effect on film properties, such as thickness, crystallinity, and electronic properties. [6]

Zirconium and zirconium alloys form a strongly adherent, protective ZrO_2 film in most media. This passive film gives zirconium excellent corrosion behavior in most solutions. [2] In water, the oxidation reaction for zirconium alloys is: [10]

$$Zr + 2H_2O \text{ -----} > ZrO_2 + 2H_2 \quad (2\text{-}4)$$

Zirconium remains passive, and corrosion resistant, in most acids, including hydrochloric acid, nitric acid at below 98% concentration, sulfuric acid below 70% concentration, phosphoric acid below 55% concentration, and chromic acid at less than 30% concentration. [2] These results were determined using immersion tests, at the

boiling temperature for each solution. [2]

Zirconium stays passive in most alkalies, including sodium, potassium, calcium and ammonium hydroxides.[1,2]

Zirconium remains passive in most aqueous salts, including sodium, potassium and calcium chlorides. [2]

Zirconium stays passive in most non-halogen containing organic compounds, including organic acids, alcohols, urea, and terphenyls. [2]

2.1.3.3 Passivity Breakdown

Passivity breakdown generally occurs in the presence of aggressive ions, such as chloride or fluoride.[7] Films can break down due to several mechanisms, such as dissolution, mechanical failure, or electronic breakdown. [8,9]

Dissolution occurs when the passive film formed is attacked by the solution, and is generally followed by repassivation or preferential dissolution, such as pitting. Mechanical breakdown occurs in very thick films, when stresses caused by film formation cause film fracture. [11] With zirconium, such stresses are compressive, and mechanical failure has been demonstrated on zirconium oxide films that were grown slowly. [11]

In nitric acid at high potentials, zirconium is susceptible to stress corrosion cracking. [2] The passive film formed on zirconium can be broken down by aggressive halides. Specifically, immersion tests with oxidizing chlorides, 2% $FeCl_3$ or $CuCl_3$ showed passivity breakdown. The same is true for organic acids containing chlorides such as di- or tri-chloroacetic acids. Zirconium has a low breakdown potential in HCl and NaCl, leading to pitting corrosion. [12] For example the breakdown of the passive film formed in 1.0M NaCl can be mitigated by the addition of isopropanol at a concentration of 6.0M.

In very dry organic alcohols such as methanol, the passive film can also break down and not repassivate quickly, leading to stress corrosion cracking (SCC). [2] Addition of water inhibits SCC. [2,13] Zirconium can also show passivity breakdown in 64-69% sulfuric acid, leading to SCC. [2]

2.2 Methods of Investigating Passive Films on Zirconium

2.2.1 Electrochemical Tests

Salot et al. [10] performed electrochemical experiments on Zircaloy-4 in a 1.0M sodium sulfate solution. They took the following measurements: open-circuit potential (OCP) versus time, potentiodynamic sweep , and OCP versus time after a potentiodynamic sweep. OCP after potentiodynamic sweep increases with time, indicating growth of the passive film, based on the equation:

$$dV_{ocp} = d(FL)/dt \qquad (2\text{-}5)$$

Where:

V_{ocp} is the open circuit potential

F is the electric field strength within the film

L is the film thickness

They assumed that the zirconium film grows under a high-field type mechanism; in such a system, the film growth rate can be written as:

$$dL/dt = K \exp(BF) \qquad (2\text{-}6)$$

Where

K is the kinetic constant

$B = \alpha Zq\delta/kT$

α is the shape constant (assumed to be 0.5)

Z is the charge on the mobile species (-2 for oxygen)

q is the charge of an electron

δ is 2.7Å, the mean distance between O atoms in monoclinic ZrO_2

k is the Bolzman constant

Using this model, they concluded that zirconium films grow under high-field conditions, with an electric field varying from 1.1-1.5 MV/cm.

Potentiodynamic sweep experiments generated anodic polarization curves, demonstrating that Zircaloy-4 remains passive in this solution up to 2.0 V vs SCE. Additionally, they investigated the effect of increasing the scan rate (V/sec) for the potentiodynamic sweeps. For faster scan rates, the passive current increases linearly with scan rate, indicating that the concentration of mobile defects, such as oxygen vacancies, increase with increasing scan rate. This model was supported by measurements of OCP versus time measurements after potentiodynamic sweeps. For faster sweep rates, the decay rate of OCP ($|dV_{ocp}/dt|$) increases, indicating a larger concentration of mobile (fast) defects. [10]

Balmasov, et al. [13]performed potentiodynamic experiments using a rotating disk electrode of zirconium in 1M aqueous sodium chloride solutions, with varying concentrations of isopropyl alcohol. They found that with isopropanol concentrations of over 3.0M, a passivity was observed. At 6.0M isopropanol, this passivity was pronounced, and a transpassive transition was noted. Additionally, a linear relationship between electrode rotation speed and passive current was shown. [13]

2.2.2 Electron Microscopy

Leach and Pearson [11] investigated the crystallinity of several oxides formed on the surface of several metals, including zirconium, using transmission electron microscopy. The passive films of most metals are oxides, and are amorphous when thin. Amorphous films were determined for those films that had significant tensile stresses due

to the presence of impurities. [11] For zirconium oxide, however, they found crystalline structures for the film that showed high compressive stresses. [11]

2.2.3 Electrochemical Impedance Spectroscopy

Goosens, et al. [6] investigated the electronic properties of zirconium passive films formed in 1.0M phosphoric acid using impedance spectroscopy. By using a Mott-Schottky analysis, they showed that the film is an n-type semiconductor, with an effective donor density of 4.8×10^{20} cm^{-3}. The film thickness was 36.5 nm, with a formation potential of 12V. The growth of this film was modeled using the Point-Defect Model, discussed more thoroughly in section 2.3 [6]

2.2.4 Photoelectrochemical Impedance Spectroscopy

Goosens, et al. [6] conducted electrochemical impedance investigations on the sample while it was irradiated with sub- and super-bandgap energy photons. Films were formed in 1M aqueous phosphoric acid solutions at 12V. A xenon lamp with a monochromator was used as the light source. Super-bandgap irradiation consisted of photons with a wavelength of 200 nm (6.0eV); sub-bandgap irradiation was 320nm (3.9eV). These experiments led to a model equivalent circuit with two resistor/capacitor pairs, as shown in Figure 2-1. The second resistor/capacitor pair (R_2/C_2) represents the photoelectron/photohole pair formed by the super-bandgap irradiation. The results of these experiments were modeled using the point-defect model. [6]

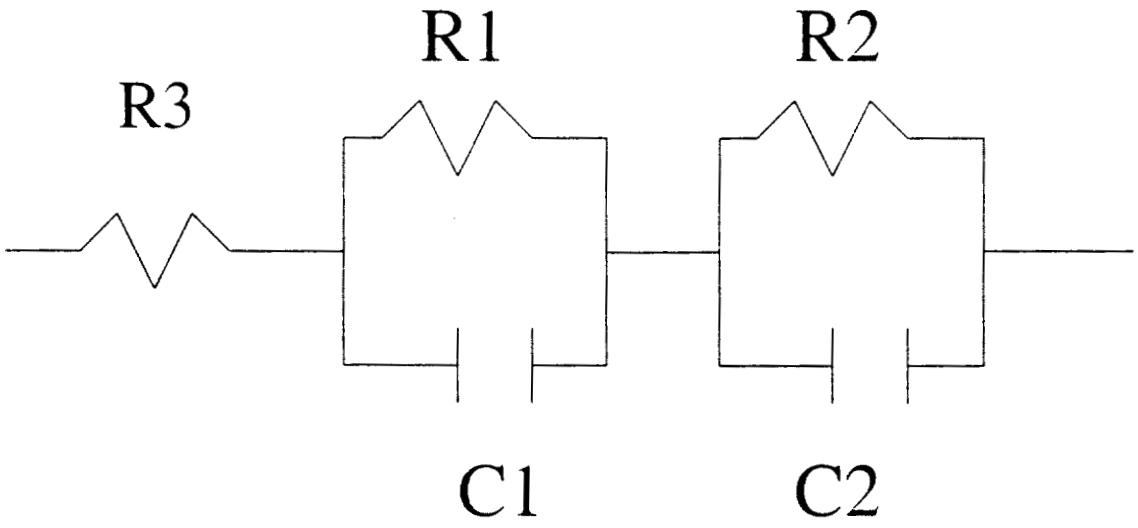

Figure 2-1. Schematic Equivalent circuit for PEIS experiments (after Goosens, et al. [6])

2.2.5 Other Methods

Khalil, et al. [14] used radiotracers to determine the transport numbers for zirconium and oxygen in passive films formed on zirconium. The electrolytes used were 0.05M NaOH, 0.044M $NH_4HB_4O_7$, and 0.05M Na_2SO_4, at potentials up to 200V. They concluded that the metal and oxygen transport numbers t_m and t_O are dependant on the current density and the electrolyte, but not on the oxide thickness. An increase in current density leads to an increase in t_m. Additionally, t_m increases when there is incorporation of electrolyte ions into the film. [14]

Goosens, et al. [6] used a number of photo techniques in their investigation of zirconium passive films formed in 1M phosphoric acid at 12V. These included measuring stationary photocurrents, photocurrent transients, and photocurrent voltammograms. Using these methods, they determined that irradiation of the sample surface stimulated film-growth due to photoquenching the electric field within the film, caused by the formation of hole/electron pairs. [6]

2.3 The Point-Defect Model

Chao, et. al [16] modeled the transport of ions and vacancies during the formation of a passive film. The assumptions of the point-defect model are:[15,16]

1) a continuous passive film will form on the surface of the metal for external potentials higher than the Flade potential;
2) the film contains a high concentration of point defects;
3) the film acts as an incipient semiconductor, on the verge of electric breakdown;
4) within the film, electrons and holes are at equilibrium, thus any electrochemical reaction involving electrons or holes are rate-limited at the film-solution or metal-film interface.

These assumptions result in the following equation, on which the model is based:

$$dL/dt = (\Omega/N_v)\, J_{VO^{\cdot\cdot}} \qquad (2\text{-}7)$$

Where

L is the film thickness

Ω is the molar volume per cation

N_v is Avogadro's Number

$J_{VO^{\cdot\cdot}}$ is the flux of oxygen vacancies per unit time

Integrating with respect to time gives a simplification of the form:

$$\exp(2KL) - 2KL - 1 = 2KA(B-1)t \qquad (2\text{-}8)$$

Where:

L is the film thickness

K is $F\varepsilon/RT$

t is the time

A,B are constants

2.4 Electronic Properties of Passive Films

It has been found that thin passive oxide films on most metals are non-crystalline. As their thickness increases, they become more crystalline, probably due to the high stresses caused by their growth. [11] The presence of crystallinity in passive films may change their electronic properties, and thus their corrosion behavior. [9] The chemical and structural properties of the passive film, in terms of the transport of ions and electrons through the film, determines the dissolution and breakdown of the film. [8]

In semiconductors, electrons fall into one of two bands: the conduction and valence band. The energy gap between these two bands is called the bandgap energy (E_g). Defects in semiconductors are either n-type (contributing electrons to the conduction band), or p-type (accepting electrons from the valence band). This is illustrated in Figure 2-2. Depending on the type of defect in the film, passive films may be p- or n-type semiconductors, or can be insulators.[8] Insulators include such films as Al_2O_3 in the form of corrundum[9]; n-type films include TiO_2, TiN and Fe_2O_3; p-type films include FeO, Cr_2O_3, MnO and CuS. [17,18] Donor densities in the passive film on iron, for example, can be as high as 10^{20}-10^{21} cm^{-3}. [19, 20] Alloying elements can act as dopants in the film as well. [21] For example, in Fe-Cr alloys, the Cr acts as an n-type dopant. [22]

Film formation potential also has an effect on the defect structure of passive films. Passive films formed on iron at higher potentials show lower defect concentrations than those formed at lower potentials. [23]

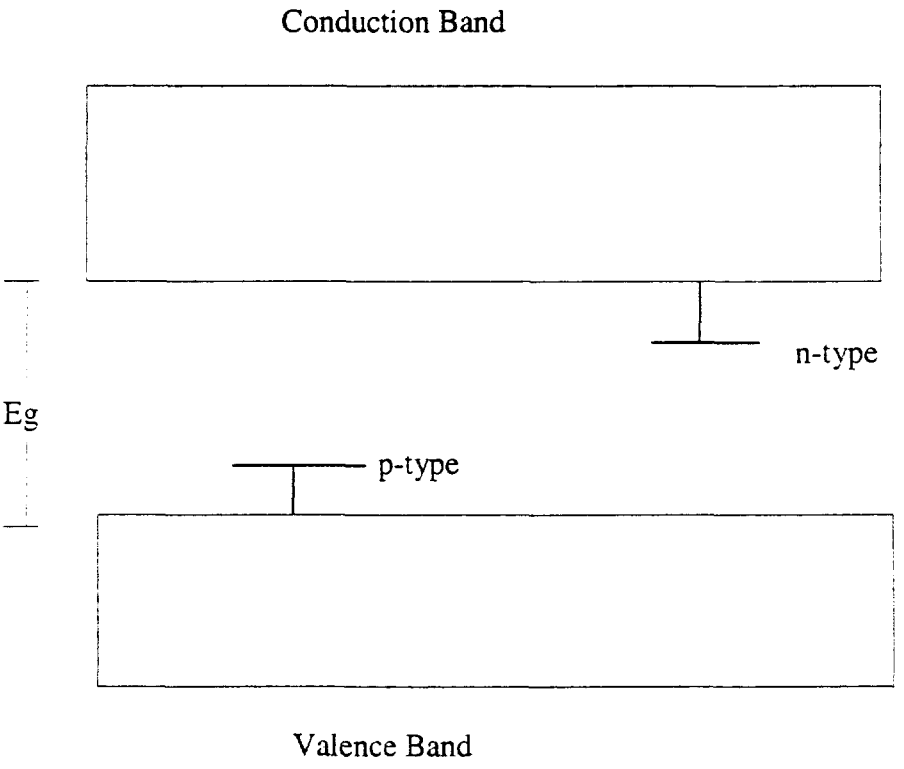

Figure 2-2. Electron energy levels in semiconductors

When a potential is imposed across a metal/film/solution system, a charge distribution develops. The charge distribution in the film is called the space-charge layer. The potential within the film at which electrons and holes are in equilibrium is called the flatband potential (E_{fb}). In the solution, the charge distribution forms the electric double layer, ending at the Outer Helmholz Plane (OHP). This is illustrated in Figure 2-3. These charges act as capacitances; the entire film/solution system has a total capacitance of:

$$1/C = 1/C_{SC} + 1/C_H \qquad (2\text{-}9)$$

Where:

C is the total system capacitance

C_{SC} is the space-charge layer capacitance

C_H is the Helmholz capacitance

Usually, $C_H >> C_{SC}$, so the total capacitance can be approximated by the space-charge capacitance. Because of this capacitive behavior, a metal/film/solution system can be modeled by a resistor in series with a parallel resistor-capacitor pair, as shown in Figure 2-4.

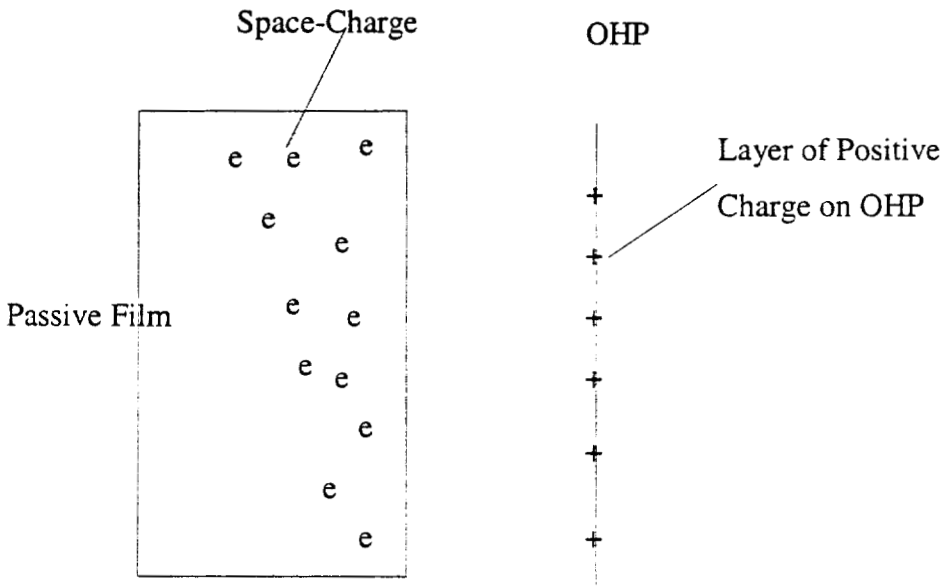

Figure 2-3. Space-charge layer and Outer Helmholz Plane

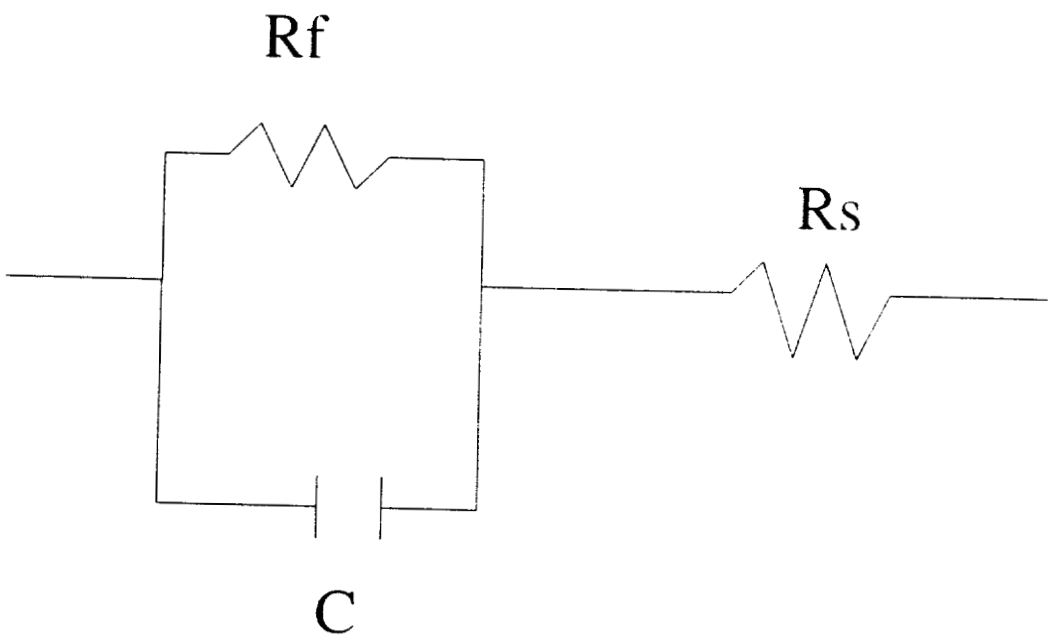

Figure 2-4. Schematic of Equivalent Circuit for Modeling Passive Films

The most direct and frequently used technique to determine the semiconducting properties of the passive film are AC Impedance studies, such as Electrochemical Impedance Spectroscopy (EIS).

The capacitance of the passive film can be measured, and those measurements can be used to determine many of the semiconductor properties of the film. Mott and Schottky determined one such relationship [24,25]:

$$1/C_{SC}^2 = [2/eN_D\varepsilon\varepsilon_0](V_m - V_{FB} - kT/e) \qquad (2\text{-}10)$$

Where:

C_{SC} is the space-charge capacitance

e is the charge on the electron

ε is the dielectric constant

ε_0 is the permittivity of free space

N_D is the donor density

V_m is the imposed potential

V_{FB} is the flatband potential

k is the Bolzman constant

T is the absolute temperature

Using the definition of total capacitance, (2-9, above), this can be written as:

$$1/C^2 = 1/C_H + [2/eN_D\varepsilon\varepsilon_0](V_m - V_{FB} - kT/e) \qquad (2\text{-}11)$$

Where:

C is the total capacitance

C_H is the Helmholz capacitance

The above equations assume that the donor density is constant throughout the film. There have been some studies of Mott-Schottky curves with non-constant donor density.[26-28] Wei Su [29] calculated another form of the Mott-Schottky relationship, with a graduated donor density, from zero at the film-solution interface:

$$1/C^3 = [3/ea(\varepsilon_0\varepsilon_s)^2](V - V_{FB} - kT/e) \qquad (2\text{-}12)$$

Where:

a is the donor density gradient

ε_s is the semiconductor dielectric constant

3.0 Experimental Procedures

3.1 Justification of Experimental Techniques Used in this Investigation

3.1.1 Electrochemical experiments

Electrochemical experiments were conducted in order to understand the passivation behavior of zirconium in aqueous sulfuric acid, aqueous hydrochloric acid, and aqueous-methanolic sulfuric acid. Potentiodynamic experiments were conducted in order to develop polarization curves, to help determine the active, passive and transpassive behavior of zirconium in these electrolytes over a wide potential range. A schematic polarization curve for an active-passive metal is shown in Figure 3-1 [30] Information gained from the polarization curve includes: the presence or absence of an active (etching) range of potentials, the range of passive potentials, and the presence or absence of a transpassive region,[30] and the stability of the passive region. [31] The measured potentials depends on the solution chemistry, temperature and, in some cases, agitation, and the alloying elements in the material. [32]

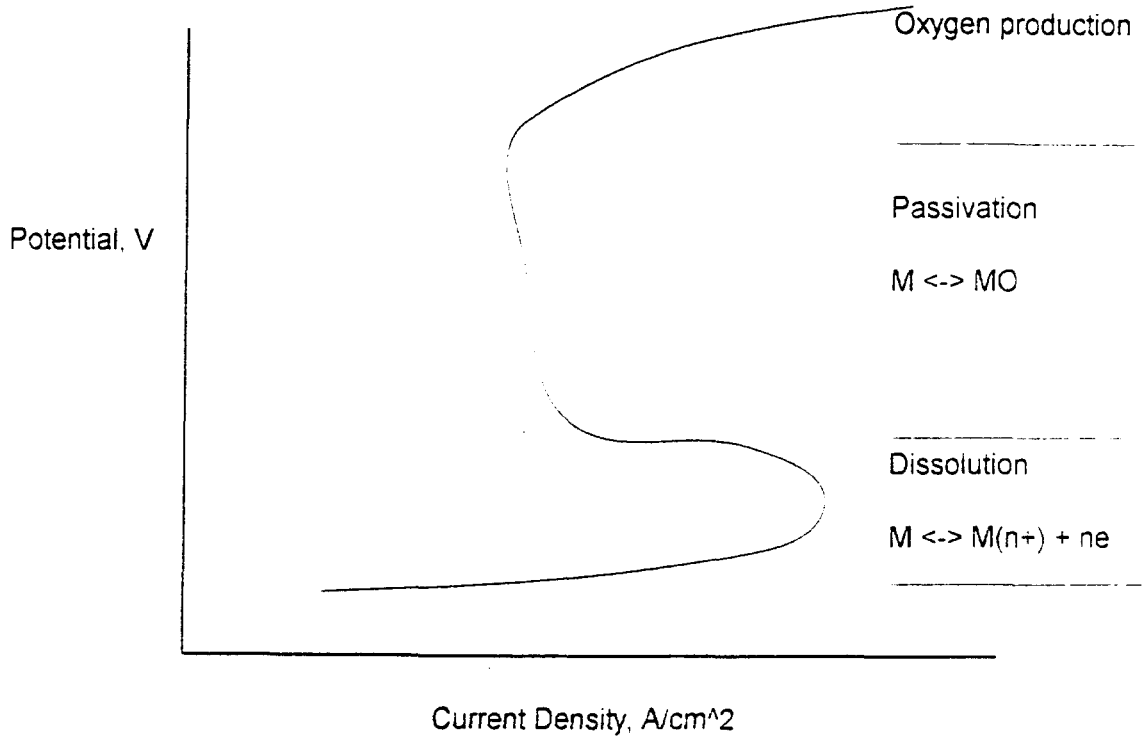

Figure 3-1. Schematic Representation of an Anodic Polarization Curve for an Active-Passive Material

Potentiostatic experiments were conducted at potentials within the passive region, selected using these polarization curves. Potentiostatic experiments allow the growth of passive layers for examination using the techniques described below. Current versus time (I vs t) curves were obtained during potentiostatic experiments.

3.1.2 Optical and electron microscopy

After potentiostatic experiments, the samples were examined microscopically, in order to determine whether there was any localized corrosion, or precipitation on the sample. Optical microscopy and SEM were used.

3.1.3 SEM/EDS

Scanning electron Microscopy (SEM) was used to study the surface features of passive films. [6] Electron Dispersive Spectroscopy (EDS) is an analytical method used in conjunction with an SEM to determine the chemical composition of the passive films. It operates by focusing a beam of electrons on the surface of the sample, and collecting and measuring the x-ray energies emitted by the atoms in the sample. Collecting and measuring these energy spectra was used to quantitatively determine the atomic percent for each element present in a material.

3.1.4 X-Ray Photoelectron Spectroscopy (XPS)

XPS was used to determine the chemical composition and thickness of the passive films formed potentiostatcially. XPS works by projecting a monoenergetic beam of X-rays at the surface, and measuring the energy of photoelectrons ejected from the atoms in the sample. This analytical method allows the determination of what kind of atoms are in the sample and their quantity, but also allows determination of the oxidation state and chemical bonds of the atoms in the film. [33] Additionally, by the use of an argon sputter, XPS can be used to determine the atomic percentage of each element in a sample as a function of depth, allowing the investigation of chemical changes within the passive film as a function of depth.[34,35] Such an investigation could show, for example, the

penetration of oxygen or electrolyte ions into the passive film as a function of depth.[35]

3.1.5 Electrochemical Impedance Spectroscopy (EIS)

EIS is used to determine the semiconducting properties of the passive films formed potentiostatcially. [36] An AC potential (with or without a DC bias) is applied to the sample, and the resulting current is measured.[37] A passive film can be modeled as a resistor in series with a parallel resistor/capacitor pair as shown in Figure 2-4, and EIS can be used to find the values of these resistance and capacitance. [38] Frequencies for EIS can range from 10^{-4} to 10^{6} Hz.

3.2 Materials and Specimen Preparation

For the electrochemical experiments, the specimens were prepared by first cutting bar stock into approximately 1.25 cm (0.5") sections. These disks were spot welded to a copper wire to provide a good electrical connection. The wire was sheathed in Nalgene tubing, and the assembly mounted in epoxy, which covered the specimen, weld joint, and approximately one cm of tubing. A schematic view of the electrochemical specimens is shown in Figure 3-1. After the epoxy had set, these specimens were ground flat, and wet-polished using 600-grit SiC paper.

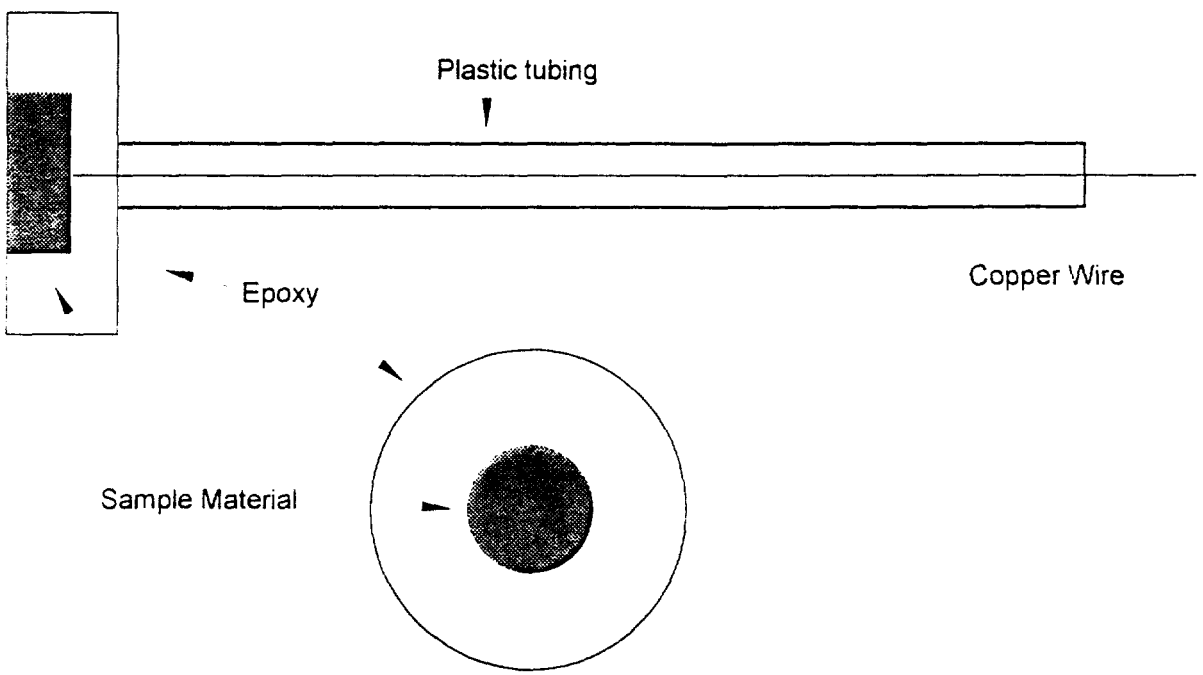

Figure 3-2. Schematic Electrochemical Specimen

For the SEM and SEM/EDS analyses, the specimen design was modified. Because the SEM requires electrical contact between the sample and the stage, the long, sheathed copper wire-type specimens could not be used. Instead, a modified specimen, using a short copper wire was developed. This specimen geometry is shown in Figure 3-2.

For the XPS analyses, the epoxy mount would prove to be a hindrance and source of potential errors, so the specimens for XPS were prepared from cut bar stock, which were polished unmounted, to a near-mirror finish using an aqueous 0.03μ SiO_2 slurry. These specimens were spot-welded to electrochemical specimens (described above), rough side down, to provide electrical contact and mechanical stability. After the potentiostatic film growth experiments, the specimens were removed, and analyzed. For EIS, the long-electrode electrochemical specimens, polished to 600 grit, were used.

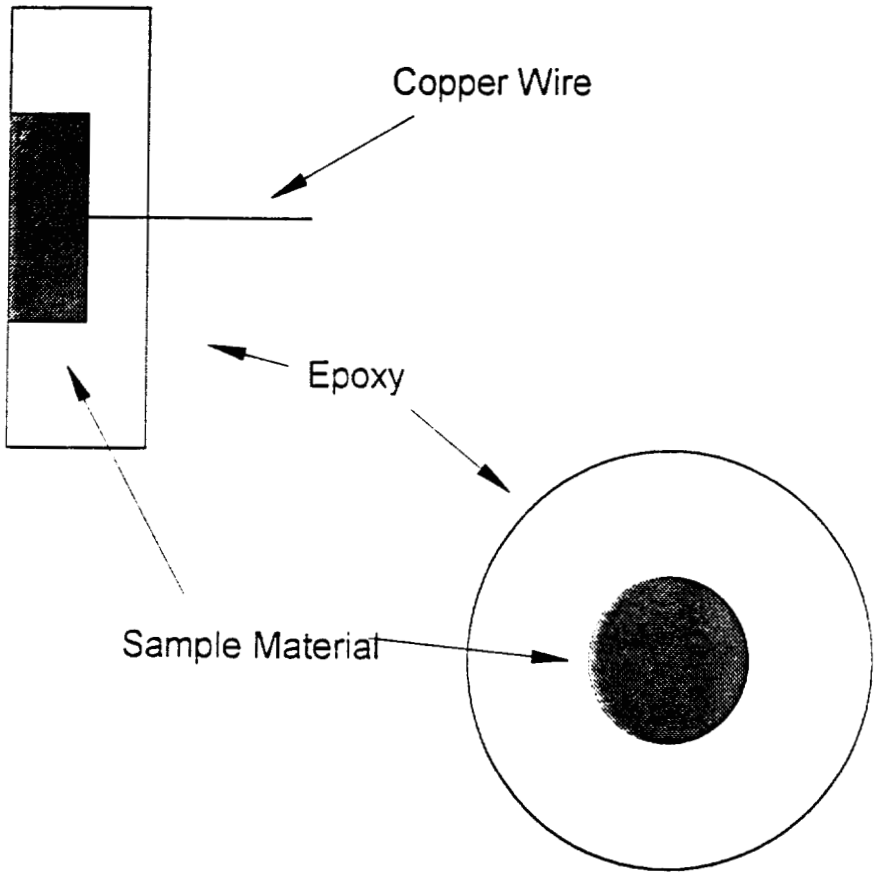

Figure 3-3. Schematic of Modified Electrochemical Specimen for SEM

3.4 Electrolyte Preparation

Aqueous solutions of sulfuric and hydrochloric acids were prepared with certified ACS grade concentrated acids and deionized water. All solutions were 1.0M in concentration. Aqueous-methanolic solutions of sulfuric acid were prepared by dilution using pure (99.99%) methanol. No precautions were taken to avoid the presence of water in the aqueous-methanolic solutions. The final water content of the 1.0M aqueous-methanolic sulfuric acid solutions was calculated to be approximately 0.5%.

3.3 Experimental Methodology

3.3.1 Electrochemical Experiments

The anodic polarization curves were generated using an EG&G model 273A potentiostat, connected to a PC for data acquisition. A three-electrode setup was used, with a platinum mesh counter electrode and a Saturated Calomel Electrode (SCE) reference electrode. A schematic diagram of the three-electrode electrochemical cell is shown in Figure 3-3. All tests were performed at room temperature, in static, non-deaerated solutions. The potentiodynamic scans began at 0.05V below the open circuit potential, and continued to 3.8V above the open circuit potential. The scan rate used in generating the polarization curves was 0.01V/sec. Experiments were halted if excessive oxygen evolution was noted from the working electrode surface, indicating that the transpassive state had been reached, or if the potentiostat's maximum current range (1 A) was approached. The parameters used for polarization curve generation are summarized below, in Table 3-1.

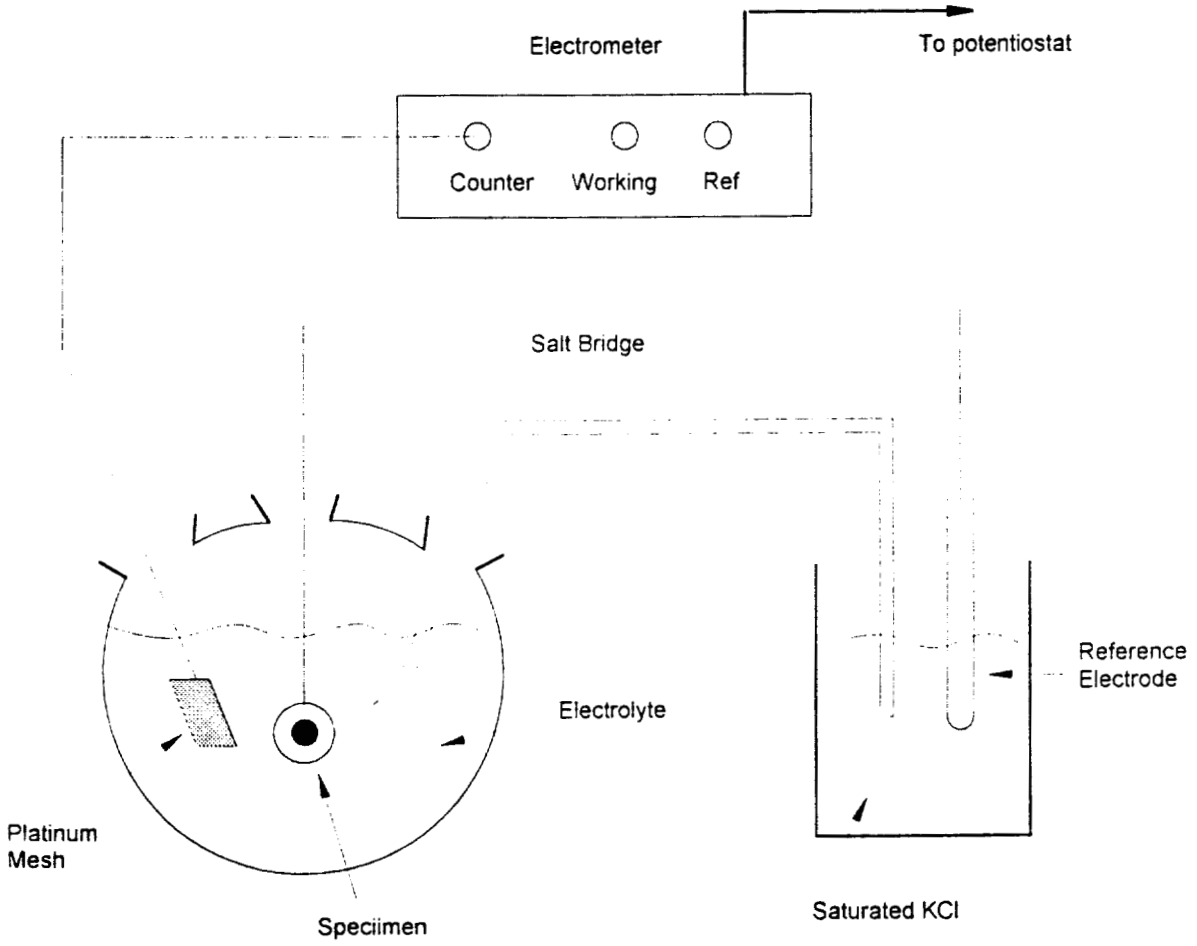

Figure 3-3. Schematic of Three-Electrode Electrochemical Cell

Table 3-1. Parameters used in potentiodynamic experiments

PARAMETER	VALUE
Cell-type	3-electrode
Counter electrode	Platinum mesh
Reference electrode	Saturated Calomel Electrode (SCE)
Starting potential	-0.05V versus open circuit potential
Ending potential	+3.8V versus open circuit potential
Scan Rate	0.01V/sec
Temperature	ambient
Solution agitation	static
Aeration	non-deaerated

The polarization curves generated using these parameters for each material in each solution were used to choose potentials for the potentiostatic film-growing experiments. Those potentials are listed in Table 4-1. Potentiostatic experiments were conducted in the three-electrode cell, using a platinum counter electrode, and an SCE reference electrode. Each specimen was held at a constant potential for 60 minutes, and the current vs time (I vs t) curves were generated. The parameters for the potentiostatic tests are summarized in Table 3-2.

Table 3-2. Parameters used in potentiostatic experiments

PARAMETER	VALUE
Cell type	Three-electrode
Counter electrode	Platinum mesh
Reference electrode	Saturated Calomel Electrode (SCE)
Potential	See Table 4-1
Time	Ten minutes
Temperature	Ambient
Solution agitation	static
Solution aeration	non-de-aerated
IR compensation	off

3.4 Optical Microscopy

After the potentiostatic experiments, the specimens were examined using optical microscopy on the Nikon Epiphot binocular microscope, in order to determine if any localized corrosion or precipitation occurred on the sample surface. Photographs were taken using the attached Polaroid camera.

3.5 Scanning Electron Microscopy (SEM)

SEM studies were conducted using a Zeiss DSM 960 SEM. SEM examination was used to determine if localized corrosion or precipitation occurred on the surface of the specimens during the potentiostatic experiments. For these studies, a beam energy of 20keV was used and the vacuum was maintained below 1 x 10^{-6} torr. The modified electrochemical specimen with a shortened, bare copper wire (Figure 3-2) were used for the SEM analyses. Images were taken both on Polaroid film and by using an image capture card, using a PC for image analysis.

3.6 Scanning Electron Microscopy/Energy Dispersive X-Ray Spectroscopy (SEM/EDS)

SEM/EDS chemical analyses were conducted using a Zeiss DSM 960 SEM. The beam energy used was 20keV, in order to allow a broad spectrum of X-ray measurements. A magnification of 200X was chosen in order to avoid measuring specific surface features (like the interiors of pits, for example), so as to better approximate the chemical composition of the entire film. The vacuum was held below 1 x 10^{-6} torr, and a no-window condition was used with the X-ray detector to allow light-element analysis and to improve sensitivity. The specimens used were the modified electrochemical specimens, with the shortened, bare copper wire. (Figure 3-2) The parameters used in SEM and SEM/EDS analyses are summarized in Table 3-3, below.

Table 3-3. Parameters used in SEM and SEM/EDS experiments

PARAMETER	VALUE
Beam energy	20keV
Vacuum	$< 1 \times 10^{-6}$ torr
Magnification	up to 2000X for surface examination; 200X for EDS analysis
Surface finish	600 grit and near-mirror
Detector window	no window

For EDS analyses, the spectra were collected and analyzed by computer. For this application, the operator determined the source element for each peak using the peak energy, comparing it to the list of known peak energies stored within the computer.

3.7 X-Ray Photoelectron Spectroscopy (XPS)

All XPS experiments were conducted at the United States Department of Energy (DOE) Research Center in Albany, Oregon. The XPS spot size used was 600μ, with a vacuum of 1×10^{-7} torr. For depth profiling, the samples were sputtered with argon ions. The etch current was 3 mA, leading to an etch rate of approximately 0.57 Å per second based on an SiO_2 standard. In addition to potentiostatically grown films, air-formed films were also analyzed using XPS. The parameters used in the XPS experiments are summarized in Table 3-4.

Table 3-4. Parameters for XPS analysis

PARAMETER	VALUE
Spot size	600μ
Vacuum	$< 1 \times 10^{-7}$ torr
Etch current	3 mA
Etch rate (vs SiO_2)	0.57 Angstroms/sec
Surface finish	near-mirror

Once the spectra were collected, they were transferred to a floppy disk for analysis on a PC. First, the survey scan was analyzed to determine what elements were present in the film being studied. Then each individual peak was examined, to determine not only what element is present, but what bonding state that element is in. This analysis was conducted by comparing peak energies with known energies, either stored in the computer, or found in the literature. Once the peaks were identified, the relative amounts of each element in the film was calculated by using the area under each peak. The calculation involves not only the peak area, but the binding energy of the element in question, and the sensitivity factor of the instrument to that element.

By using an argon ion sputter, small amounts of material were removed from the

surface of the sample. Following each sputtering cycle, another spectrum is collected. Analyzing these spectra allows the investigation of elemental concentrations as a function of depth. Depth profiling can show not only a change in concentration, but a change in ionic state as a function of depth, and thus gives many clues to the structure of the film. Depth profiling was conducted by analyzing each spectrum generated, as discussed above, during a multi-sputter analysis. The spectra generated were plotted together, as a function of depth, and the atomic percentages were plotted versus depth.

3.8 Electrochemical Impedance Spectroscopy (EIS)

Bode or Nyquist plots were generated using an assembly of an EG&G Model 273 potentiostat connected to a Model 5315 lock-in amplifier and a PC for data collection. EIS tests were conducted using the long-electrode electrochemical specimens (see Figure 3-1) All experiments were conducted in a three-electrode cell discussed above (see Figure 3-3) for the electrochemical experiments. The parameters used in generating the Bode and Nyquist plots are summarized in Table 3-6, below. [19]

Table 3-5. Parameters for Bode and Nyquist plot EIS experiments

PARAMETER	VALUE
Cell type	Three-electrode
Counter electrode	Platinum mesh
Reference electrode	SCE
Beginning frequency	0.05 Hz ($5x10^{-4}$ for some tests)
Ending frequency	15 kHz
Points per decade	10
V_0	see table 3-7
Film growth time	1 hour
Potential Amplitude	5 mV
Temperature	ambient
Solution agitation	static
Solution aeration	non-deaerated

In addition to Nyquist and Bode plots, EIS was used to determine the semiconductor properties of a passive film, using the Mott-Schottky model. [24] A full discussion of this theory is presented in the Literature Review section. To perform these tests, a constant frequency was applied, and the capacitance was measured at various potentials in the passive range for each solution. The experiments were conducted in the three-electrode cell, with a platinum counter electrode, and an SCE reference electrode. The parameters for the Mott-Schottky EIS tests are summarized in Table 3-6.

Table 3-6. Parameters for Mott-Schottky EIS tests

PARAMETER	VALUE
Cell type	Three-electrode
Counter electrode	Platinum
Reference electrode	SCE
Frequency	1 kHz
Potential range	See Table 3-7
Film growth time	1 hour
Potential amplitude	5 mV
Temperature	ambient
Solution agitation	static
Solution aeration	non-deaerated

Table 3-7. Potential ranges for Mott-Schottky EIS tests

SOLUTION	Zr-702	Zr-704
1.0M HCl	0.0V	0.0V
1.0M H_2SO_4 (aqueous)	0-3V	0-3V
1.0M H_2SO_4 (methanolic)	0.0V	0.0V

4.0 Results

4.1 Electrochemical Experiments

4.1.1 Polarization Curves

Figure 4-1 shows the anodic polarization curves for Zr-702 in 1.0M sulfuric acid and 1.0M hydrochloric acid. In sulfuric acid, Zr-702 has a broad passive region, and remains passive at 3.5V, with very low current densities. Similar results were obtained by Yau. [2] In hydrochloric acid, no passive region is observed, at a high scan rate, and the current increases steadily with increasing potential. At 1.0V, a current of approximately 1 A was reached, and vigorous bubbling of oxygen and hydrogen occurred on both the working electrode and the counter electrode, respectively. After this experiment, the specimen surface showed localized corrosion in the form of pitting, as shown in Figure 4-14.

In order to show transpassive behavior of zirconium in sulfuric acid, the solution was modified. Balsamov, et al. [13] modified the behavior of aqueous sodium chloride solutions by the addition of isopropanol. From this data, it is clear that the water content of the electrolyte directly affects the transpassive behavior of zirconium. Therefore, the water content of the sulfuric acid solution was reduced by replacing water with methanol. The resulting solution contained about 0.5% water. Figure 4-2 shows the anodic polarization curves for Zr-702 in aqueous and aqueous-methanolic sulfuric acid solutions. In the aqueous-methanolic solution, a passive region is observed, as in the aqueous solution, but there is also a transpassive region above 2.0V.

Figure 4-3 shows the anodic polarization curves for Zr-704 (Zr+1-2Sn+0.2-0.4Fe+Cr) in aqueous sulfuric and hydrochloric acids. These curves show that the corrosion behavior of Zr-704 is similar to that of Zr-702. In the sulfuric acid solution, the sample was still passive at 3.5 V, and showed no clear passive region in the

hydrochloric acid solution. A comparison of the polarization curves for Zr-704 in aqueous and methanolic sulfuric acid solutions is shown in Figure 4-4. As with Zr-702, the methanolic solution shows transpassive behavior at over two volts.

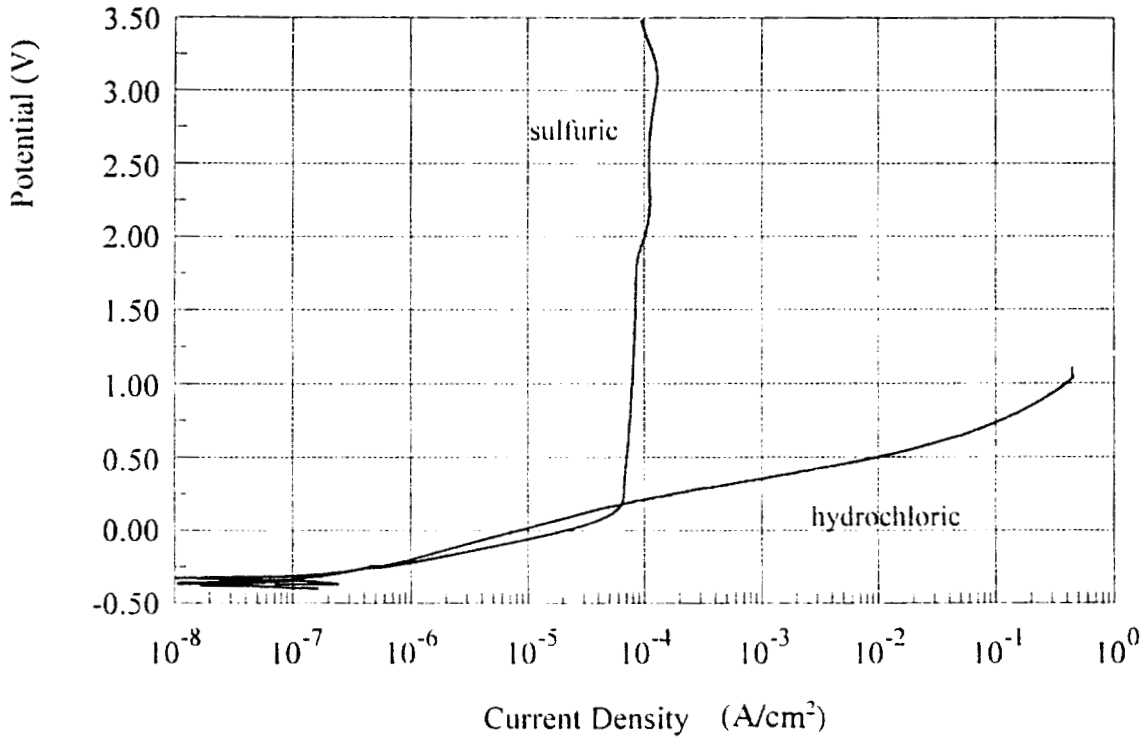

Figure 4-1. Anodic Polarization Curves for Zr-702 in 1.0M Sulfuric Acid and 1.0M Hydrochloric Acid

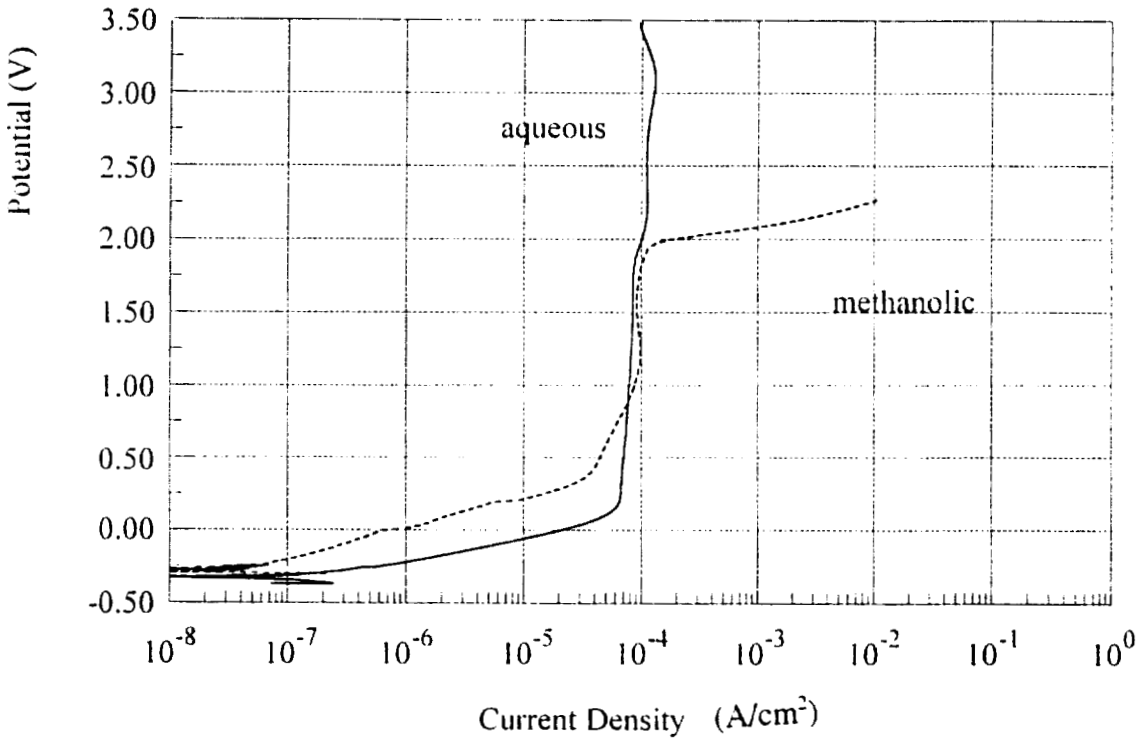

Figure 4-2. Anodic Polarization Curves for Zr-702 in Aqueous 1.0M Sulfuric Acid, and Aqueous-Methanolic 1.0M Sulfuric Acid

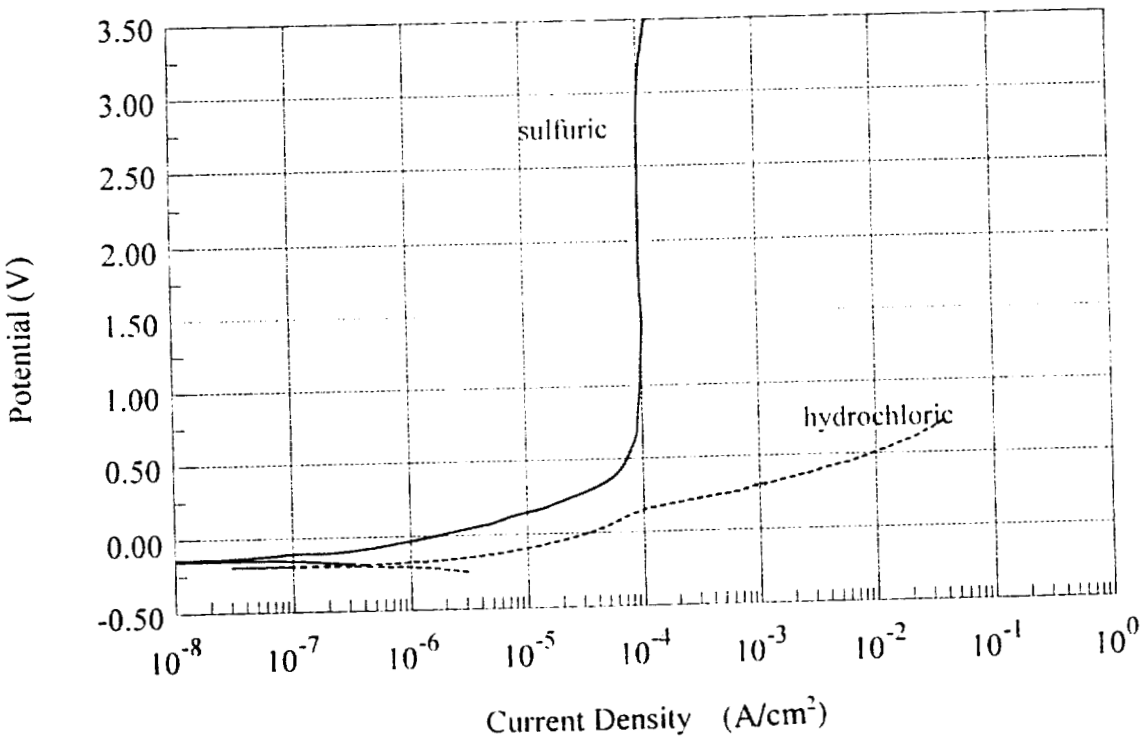

Figure 4-3. Anodic Polarization Curves for Zr-704 in 1M Sulfuric and 1M Hydrochloric Acid

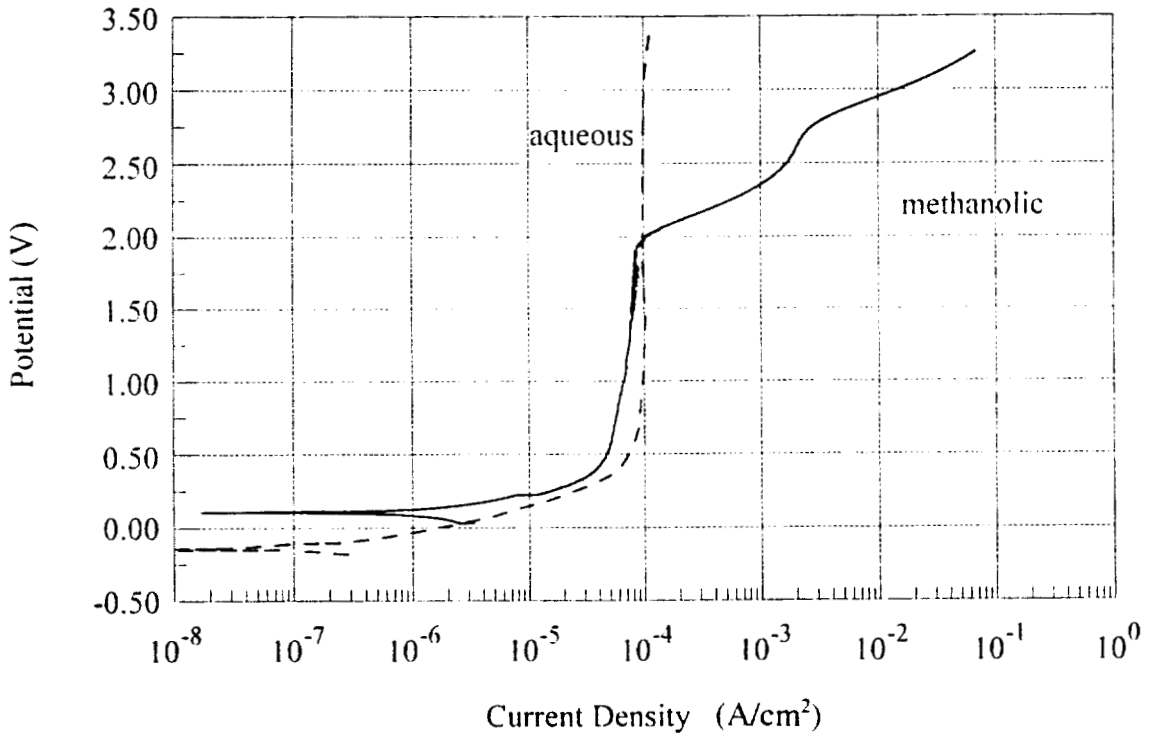

Figure 4-4. Anodic Polarization Curves for Zr-704 in Aqueous 1.0M Sulfuric Acid, and Aqueous-Methanolic 1.0M Sulfuric Acid

Based on the results of the polarization curves, the following potentials were selected for potentiostatic experiments, as shown in Table 4-1:

Table 4-1. Potentiostatic experiment potentials

MATERIAL	SOLUTION	APPLIED VOLTAGE
Zr-702	aqueous sulfuric	0V
Zr-702	aqueous sulfuric	3V
Zr-702	aqueous hydrochloric	0V
Zr-702	methanolic sulfuric	0V
Zr-704	aqueous sulfuric	0V
Zr-704	aqueous sulfuric	3V
Zr-704	aqueous hydrochloric	0V
Zr-704	methanolic sulfuric	0V

In addition to determining the effect of the water content of the solution, the effect of alloying was investigated. Figure 4-5 contains the anodic polarization curves for the two alloys in aqueous 1M sulfuric acid. Both alloys show passive behavior in this solution, at a potential of 3.5V. Figure 4-6 shows the current versus time curve for each alloy in aqueous sulfuric acid at 0V. In this figure, it can be seen that the current density (and thus corrosion rate) for Zr-704 is higher than that for Zr-702, indicating that the alloying elements increase the corrosion rate of zirconium in this solution.

Figure 4-7 compares the behavior of Zr-702 and Zr-704 in hydrochloric acid. Both alloys show very limited passive regions in this solution, if any. Figure 4-8 shows the current versus time curve for both alloys in hydrochloric acid at 0V. Once again, the current density measured for Zr-704 is higher than that for Zr-702.

Figure 4-9 shows the polarization curves in aqueous-methanolic sulfuric acid, with both alloys showing similar electrochemical behavior, including a transpassive region at over two volts.

The above data indicate that the corrosion behavior of Zr-702 and Zr-704 are very similar, with slightly higher current densities measured for Zr-704 in the potentiostatic tests. All of the measured current densities in these experiments were very low, in the $\mu A/cm^2$ range, indicating that Zr-702 does not corrode appreciably in these solutions at low potentials. In these curves, we see that the current density is highest, and thus the corrosion rate the highest in the aqueous-methanolic sulfuric acid solution.

The effect of potential is shown in Figures 4-10 and 4-11. Figure 4-10 shows the current versus time curve for Zr-702 in aqueous sulfuric acid, at 0V and 3V. As expected, the current density for 3V is higher than that for 0V. Both curves show similar trends, with current density decreasing over time. Figure 4-11 is the current versus time curves for Zr-704 in sulfuric acid at 0V and 3V, showing similar behavior to Zr-702.

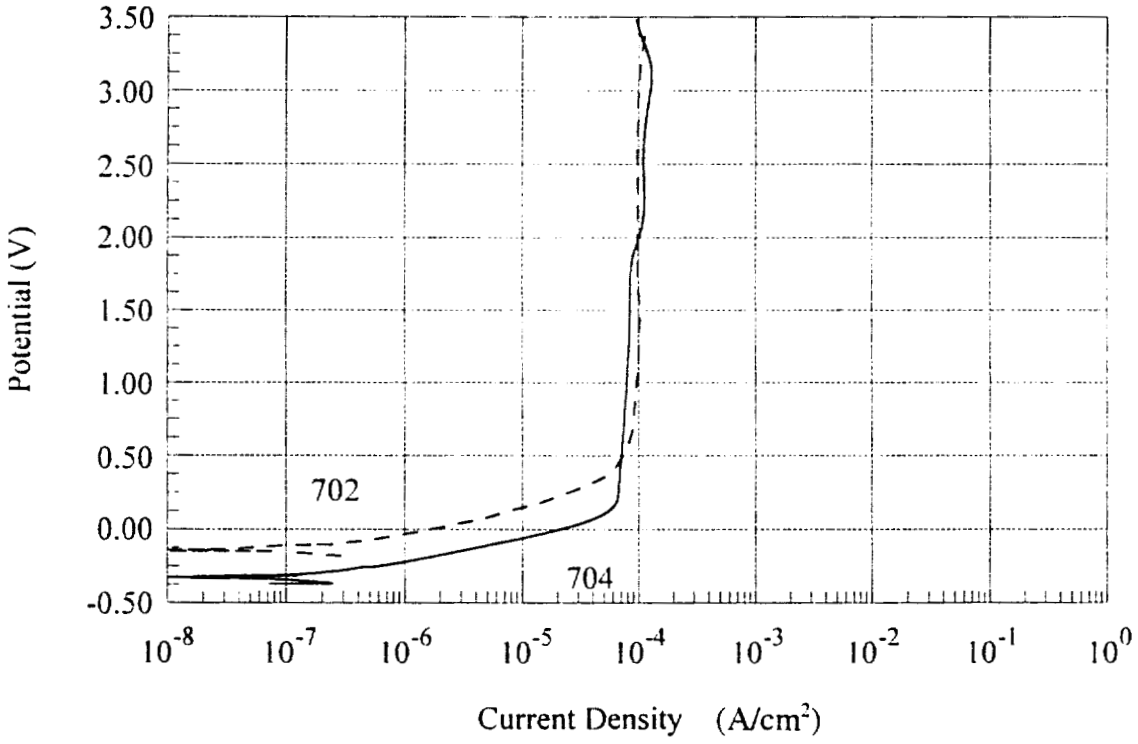

Figure 4-5. Anodic Polarization Curves for Zr-702 and Zr-704 in 1M Sulfuric Acid

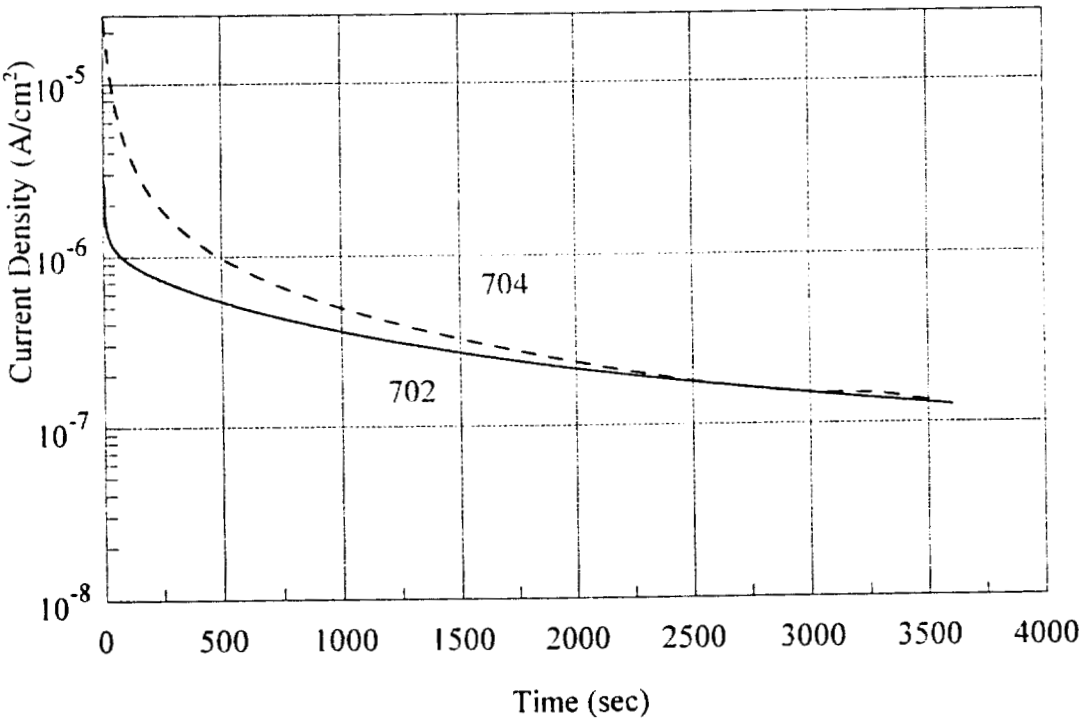

Figure 4-6. Current Versus Time Curves for Zr-702 and Zr-704 in 1M Sulfuric Acid at 0V

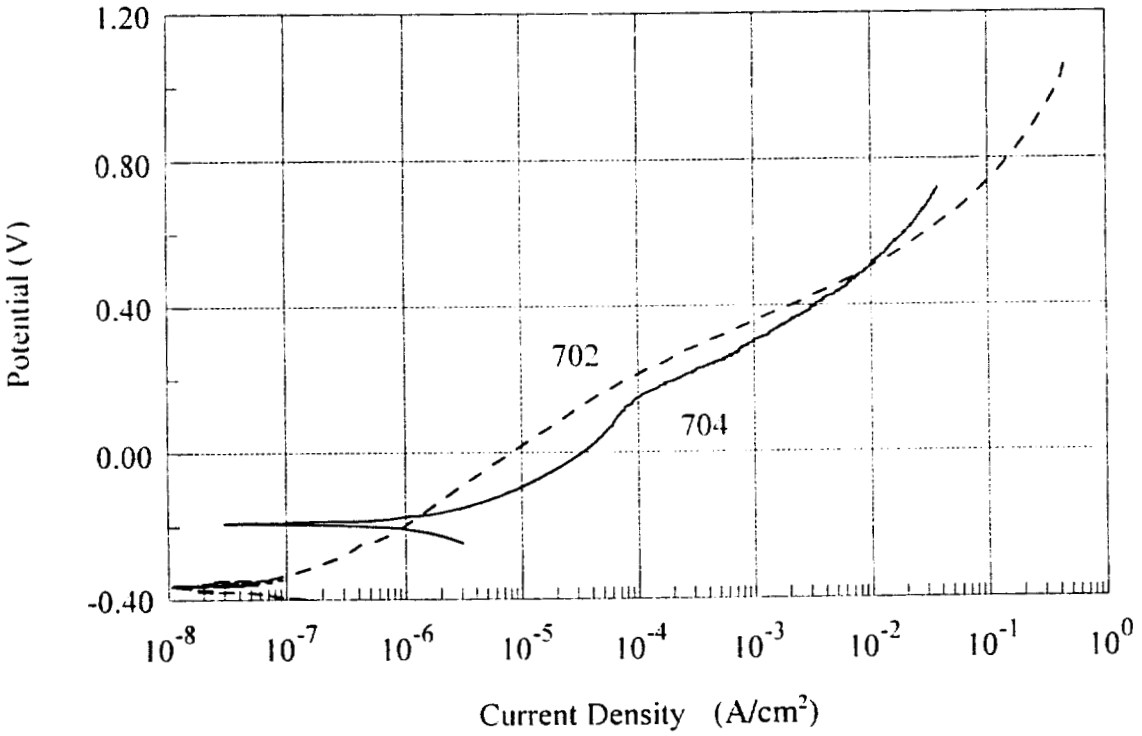

Figure 4-7. Anodic Polarization Curves for Zr-702 and Zr-704 in 1M Hydrochloric Acid

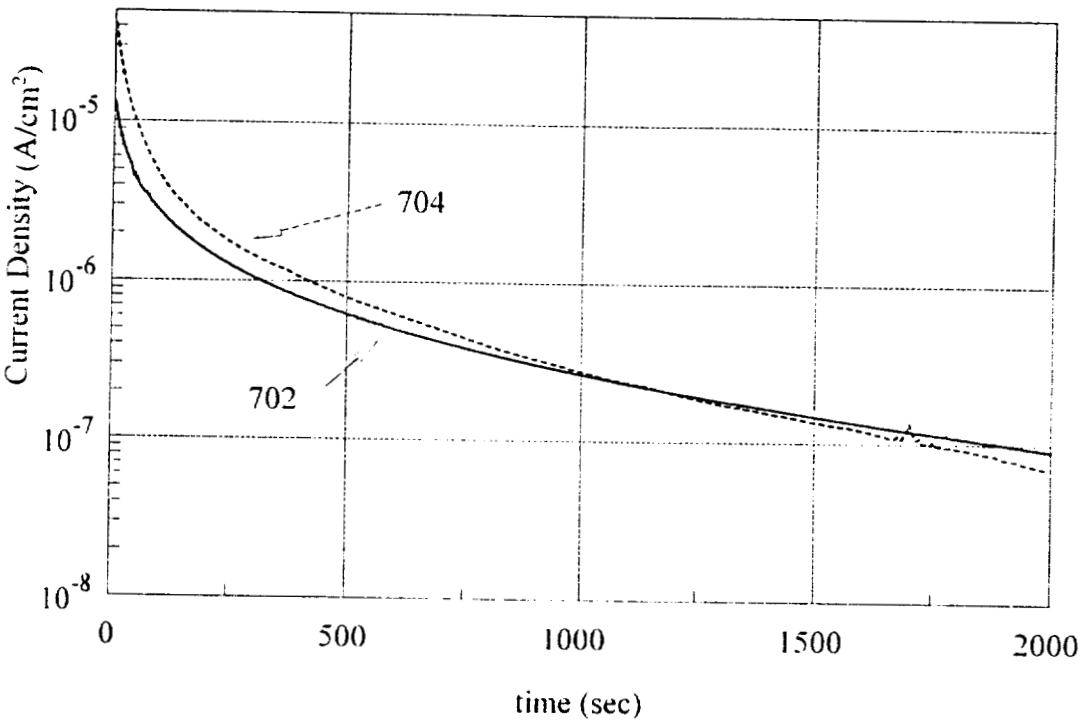

Figure 4-8. Current Versus Time Curves for Zr-702 and Zr-704 in 1M Hydrochloric Acid at 0V

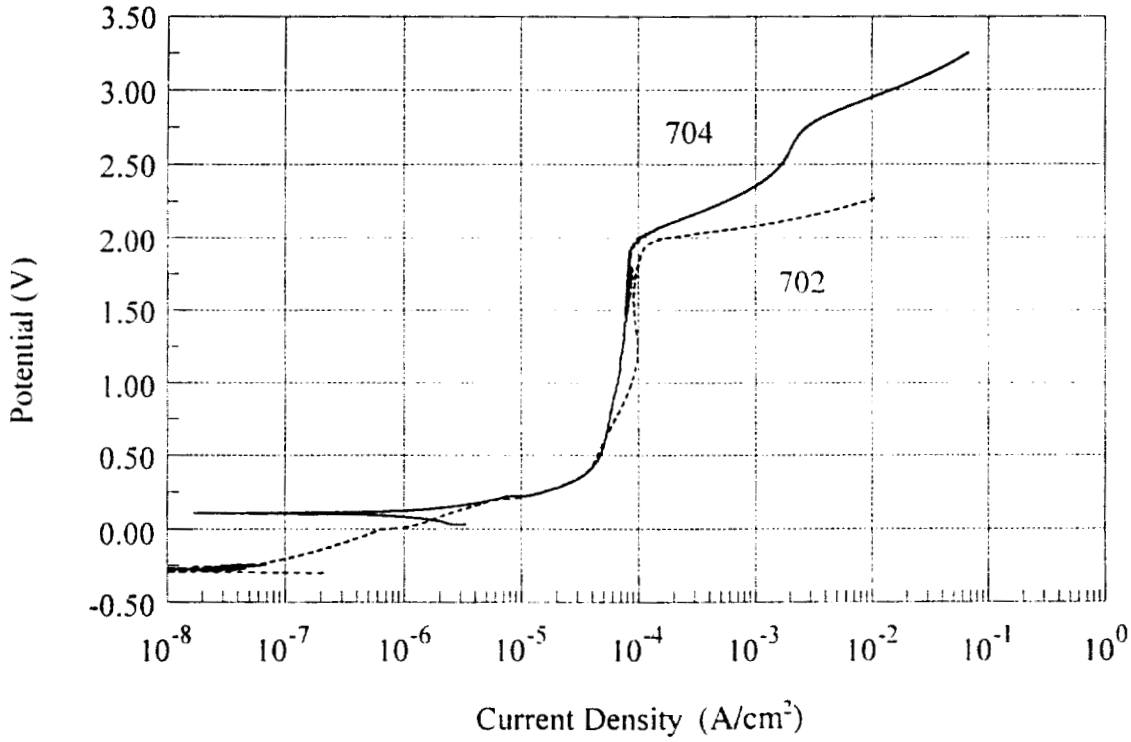

Figure 4-9. Anodic Polarization Curves for Zr-702 and Zr-704 in 1M Aqueous-Methanolic Sulfuric Acid

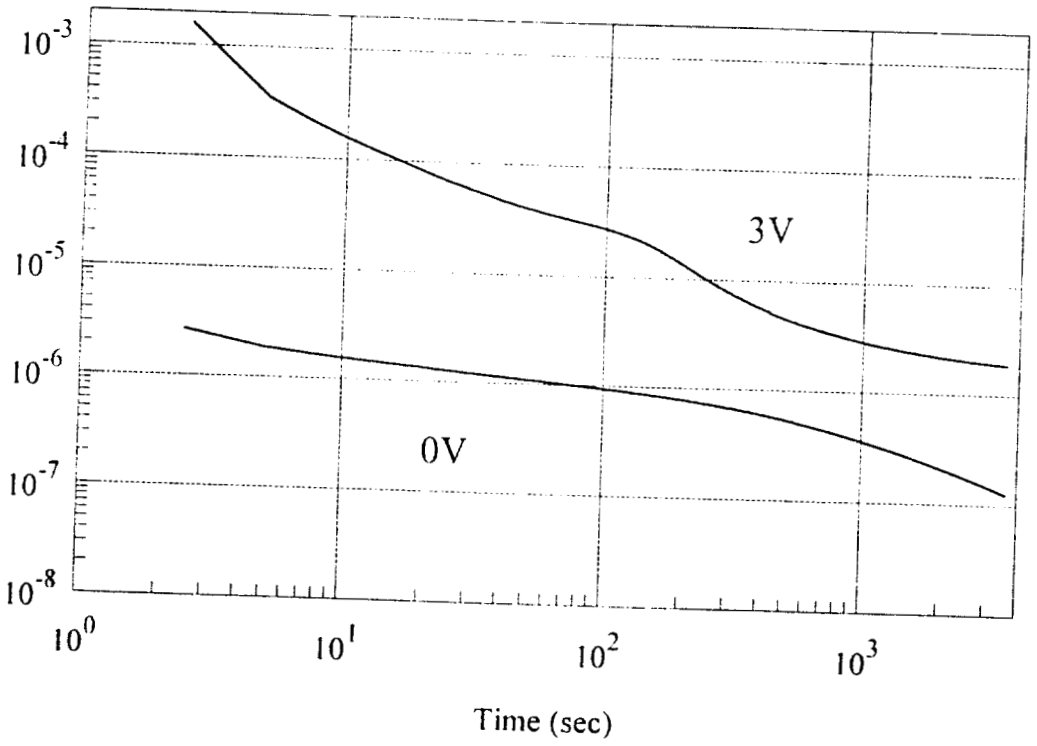

Figure 4-10. Current Versus Time Curves for Zr-702 in 1M Sulfuric Acid at 0V and 3V

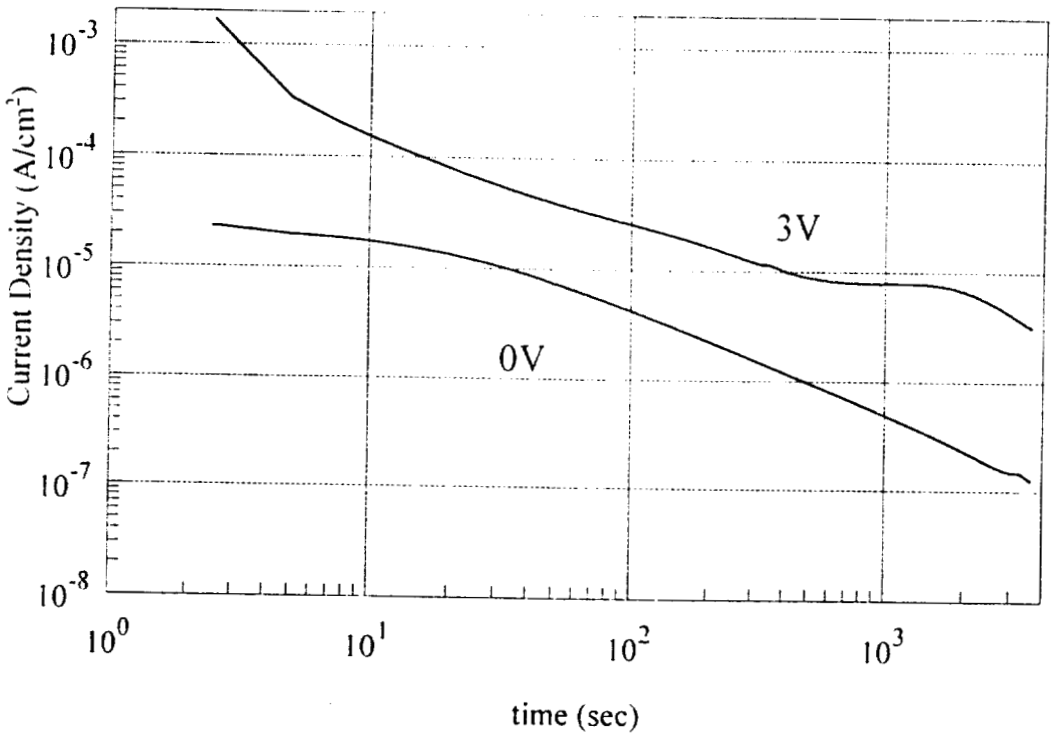

Figure 4-11. Current Versus Time Curves for Zr-704 in 1M Sulfuric Acid at 0V and 3V

4.2 SEM

Figure 4-12 shows the surface of a Zr-702 specimen, polished to a mirror surface. Scratches in the surface were used as landmarks in order to be able to focus the SEM, and these scratches appear in these figures. Figure 4-13 shows the surface of the same specimen after the potentiostatic experiments in aqueous sulfuric acid at 3V for 5 minutes. The surface is unchanged from the previous specimen. Figure 4-14 shows an SEM micrograph of a pit formed on the same sample during the potentiostatic experiments in hydrochloric acid at 0.5V.

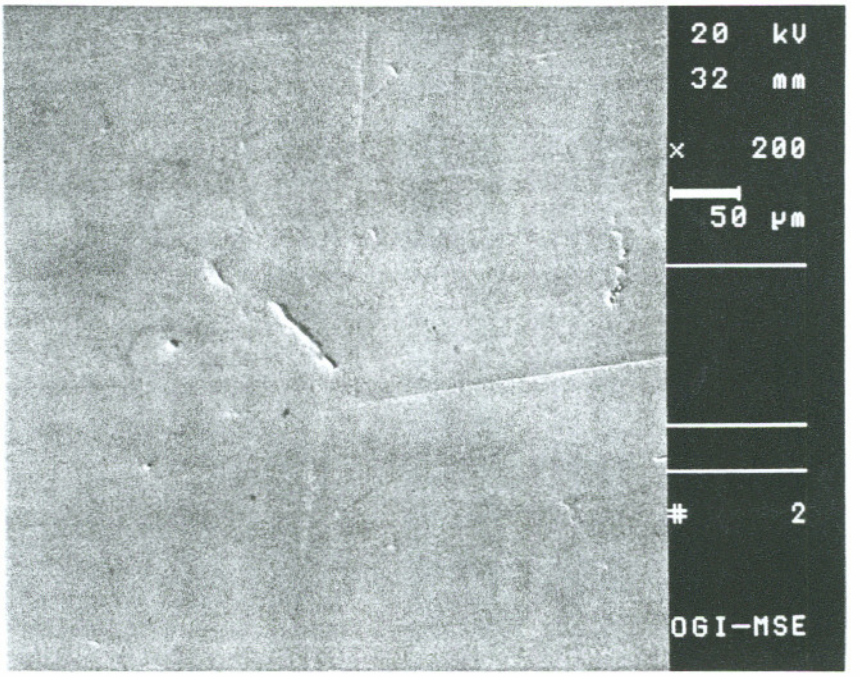

Figure 4-12. SEM Micrograph for Zr-702 Specimen

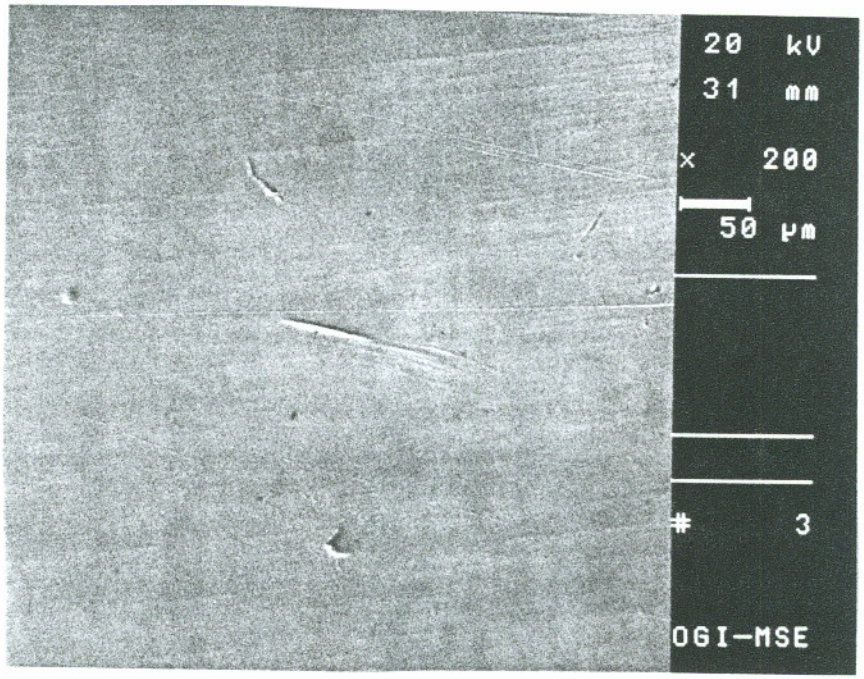

Figure 4-13. SEM Micrograph for Zr-702 Specimen after Potentiostatic Experiment in 1M Sulfuric Acid at 8V

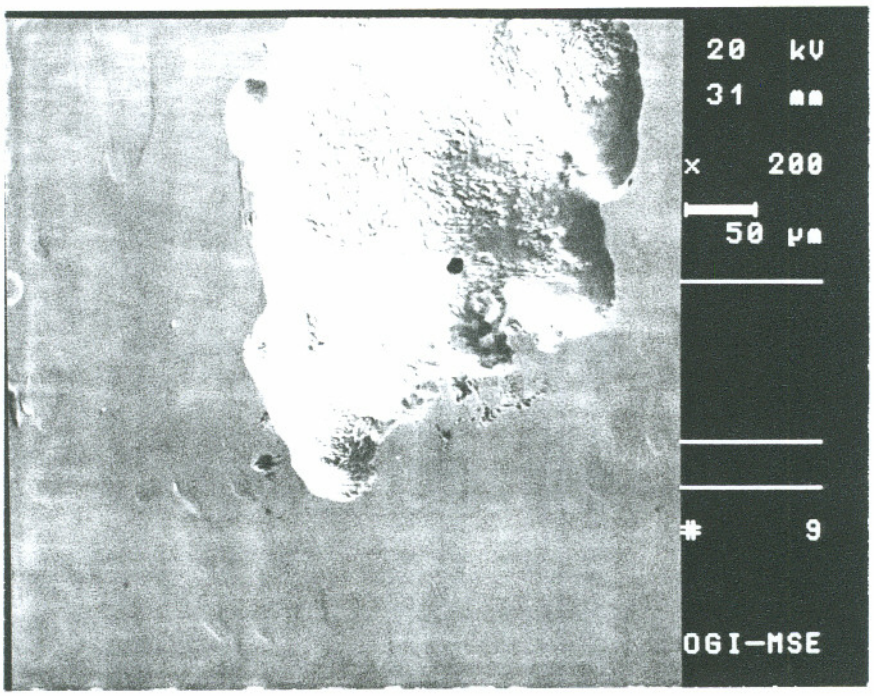

Figure 4-12. SEM Micrograph for Zr-702 Specimen after Potentiostatic Experiment in 1M Hydrochloric Acid at 0.5V

4.3 SEM/EDS

The goal of the EDS analysis was to determine if any uptake of sulfur occurred during the potentiostatic experiments. Figure 4-15 is an EDS spectrum from an air-formed film on Zr-702. The spectrum shows peaks for only zirconium and oxygen. Figure 4-16 is an EDS spectrum from a Zr-702 sample, after potentiostatic experiments in aqueous sulfuric acid at 8V. The high potential was used to grow a relatively thick film. This spectrum also shows only a zirconium and an oxygen peak. The presence of sulfur cannot be easily detected using this method, because the main sulfur peak occurs near the same energy as the zirconium peak.[39] This inability of EDS to detect sulfur lead to the use of XPS for the chemical analysis of the passive films formed.

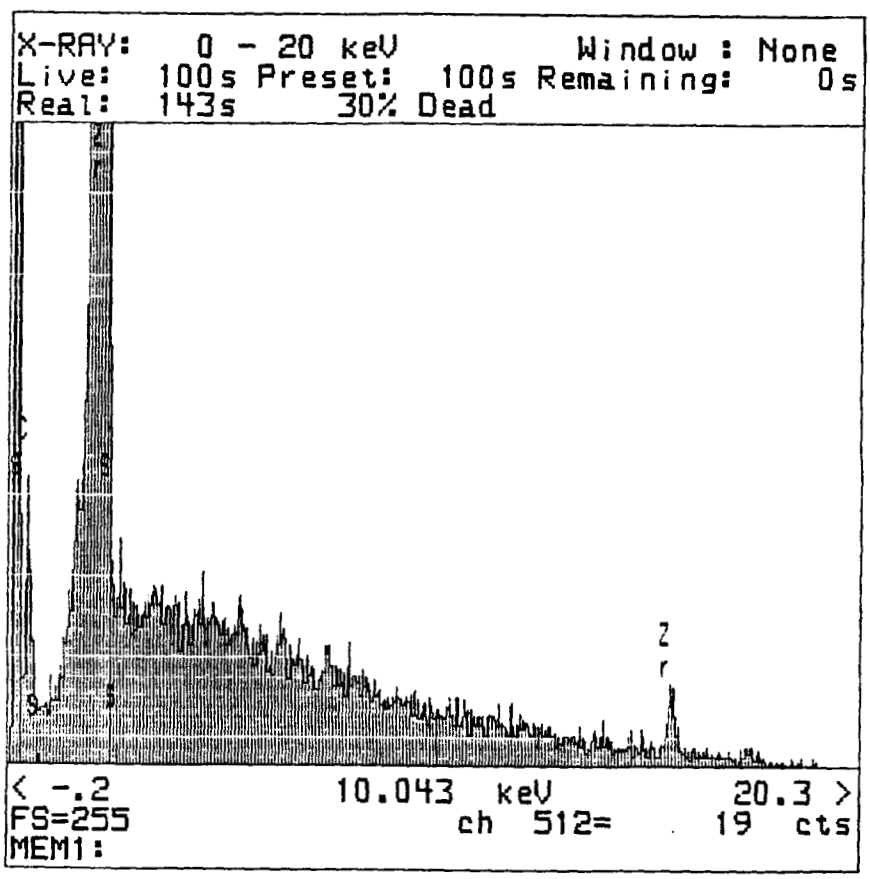

Figure 4-15. EDS Spectrum for Zr-702 Air-Formed Film

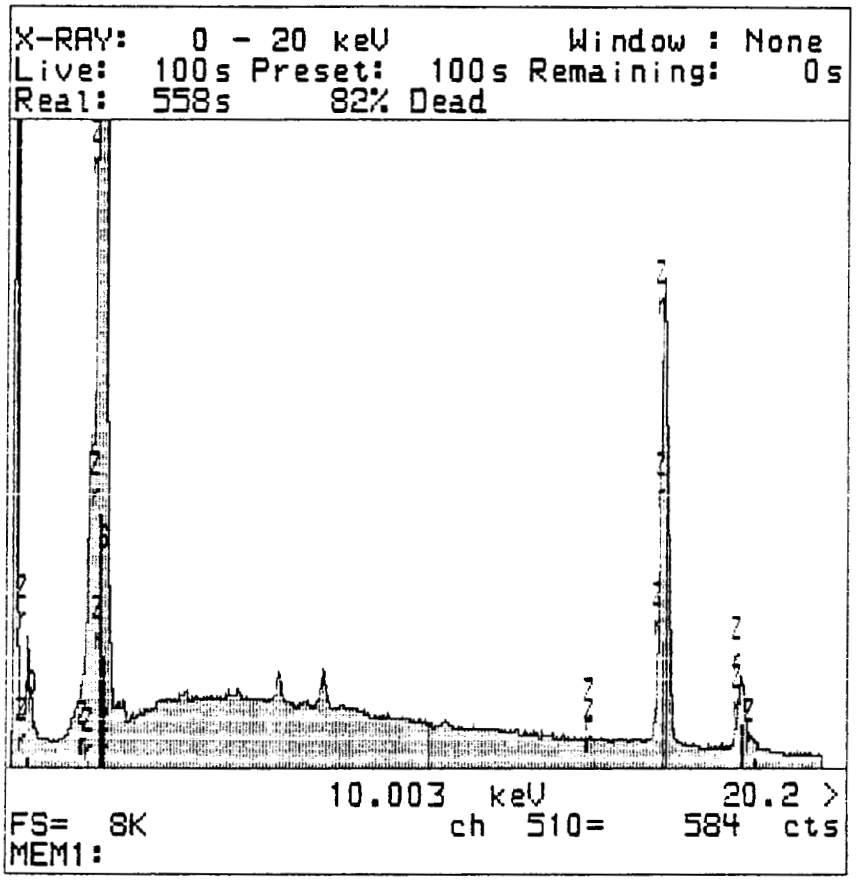

Figure 4-16. EDS Spectrum for Zr-702 After Potentiodynamic Experiment in 1M Sulfuric Acid at 8V

4.4 XPS

4.4.1 Spectra

XPS analyses were conducted at the DOE Albany Research Center. Figure 4-17 shows the surface scan taken from the air-formed film. Figure 4-18 shows the spectrum from the surface of the film formed on Zr-702 in aqueous sulfuric acid at 3V. This spectrum shows the presence of zirconium, oxygen, nitrogen and carbon. No sulfur or chlorine was detected in any scan. The nitrogen peak can be explained by the absorption of atmospheric nitrogen; the amount of nitrogen in any sample never exceeded 1%, and has not been considered in this analysis. Carbon, however, is shown at relatively high concentrations in the surface scans. Because this carbon contamination occurs even in samples where there is no carbon present in the electrolyte, this carbon is considered a contaminant, and is not considered.

Figure 4-19 shows the 3d3 and 3d5 peaks for zirconium in the metal and ZrO_2 (4+) states. This shift in peak energy allowed the determination of the oxidation state of zirconium within the sample.

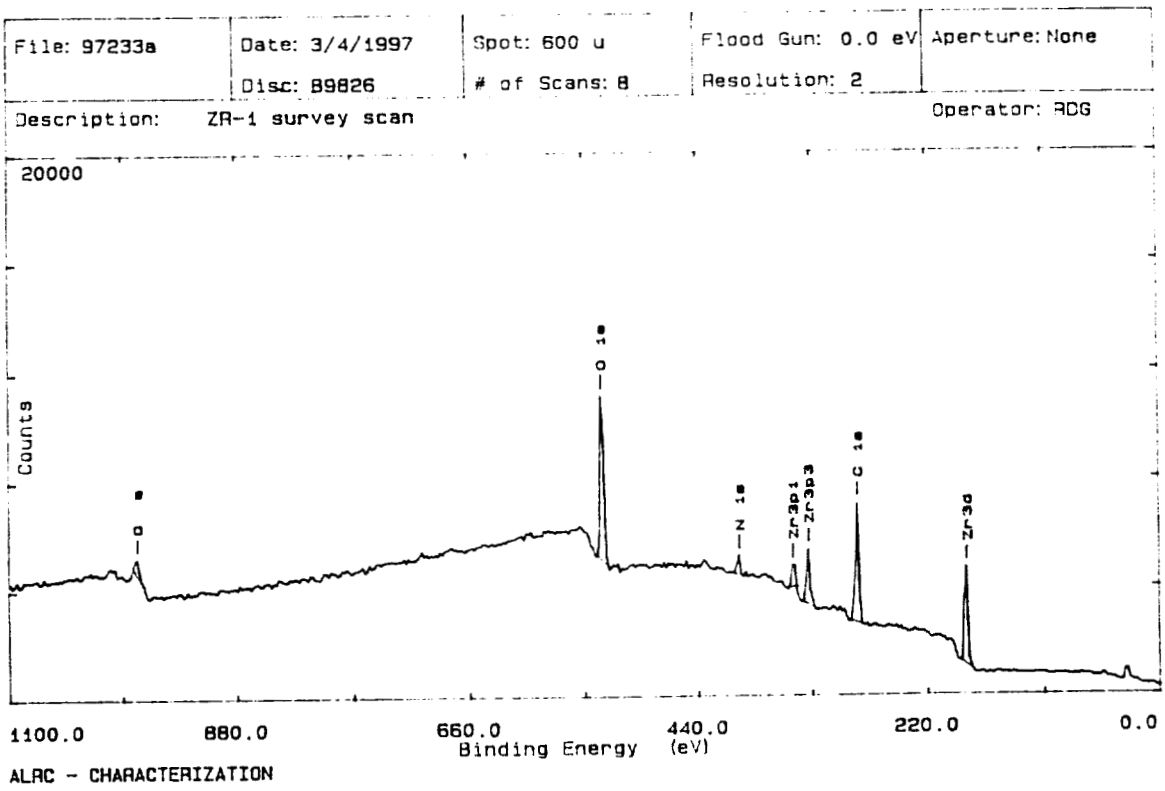

Figure 4-17. XPS Surface Scan for Zr-702 Air-Formed Film

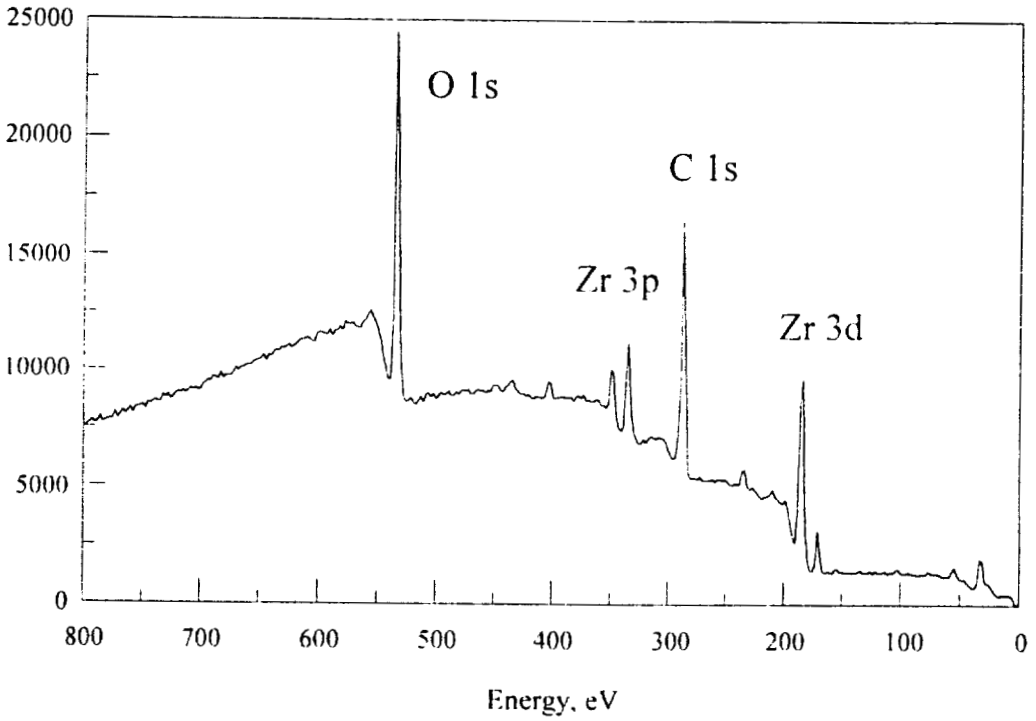

Figure 4-18. XPS Surface Scan for Zr-702 after Potentiostatic Experiment in 1M Sulfuric Acid at 3V

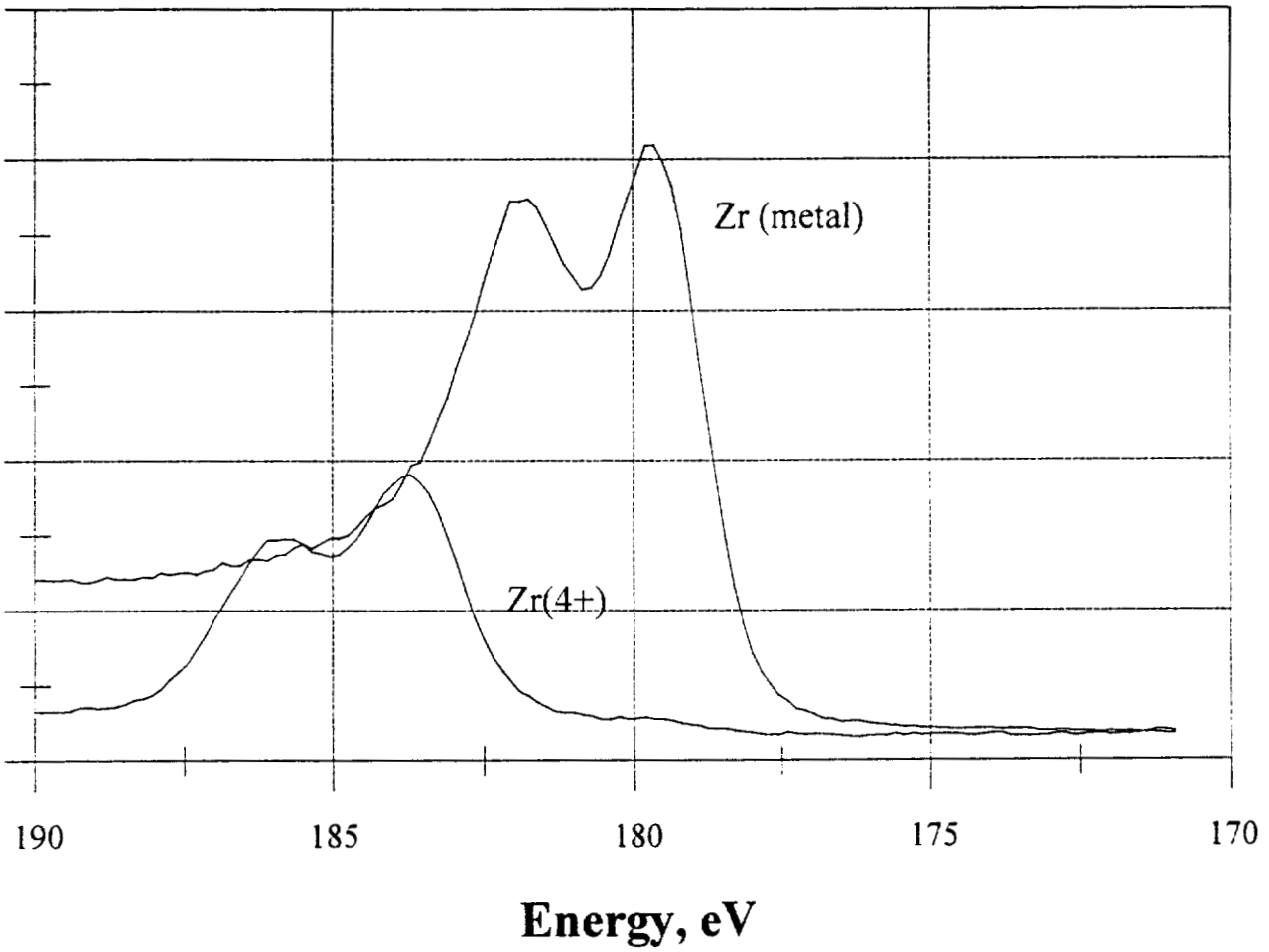

Figure 4-19. XPS Energy Spectrum for Zr 3d3 and 3d5 Peaks

4.4.2 Depth profiling

Using argon ion sputtering, several spectra were taken, with an ion sputter between each measurement. In this way, the depth profile of each element was measured. Figure 4-20 shows the atom percent measured for zirconium, carbon and oxygen for the passive film formed on Zr-702 in air. This figure shows a surface contamination of carbon of approximately 30%. As discussed in section 4.4.1, this carbon contamination can be ignored. Removing the carbon and renormalizing the atom percent leads to the distribution shown in Figure 4-21. For the purposes of this research, a characteristic thickness of the oxide film is measured by determining the depth at which the Zr:O ratio is 1:1. At this point, the film consists of half ZrO_2 and half Zr metal. For the air-formed film, this depth is approximately 30 angstroms. The depth profiles for Zr-702 in hydrochloric acid at 0V are shown in Figure 4-22. The characteristic thickness of this film is 30 angstroms, indicating that no additional film growth had occurred after the air-formed film. Figure 4-23 shows the depth profile for the film formed on Zr-702 in sulfuric acid at 0V; the characteristic thickness of this film is approximately 70 angstroms, indicating that significant passive film growth occurred during the potentiostatic experiment. Figure 4-24 shows the depth profile for the passive film formed on Zr-702 in sulfuric acid at 3V. The characteristic thickness for this film is approximately 120 angstroms, showing considerable film growth during the potentiostatic experiments. A summary of these results is shown in Table 4-2.

Table 4-2. Characteristic Depth Measured by XPS

Solution	Potential	Characteristic Depth
air-formed film	N/A	30Å
hydrochloric acid	0V	30Å
sulfuric acid	0V	70Å
sulfuric acid	3V	120Å

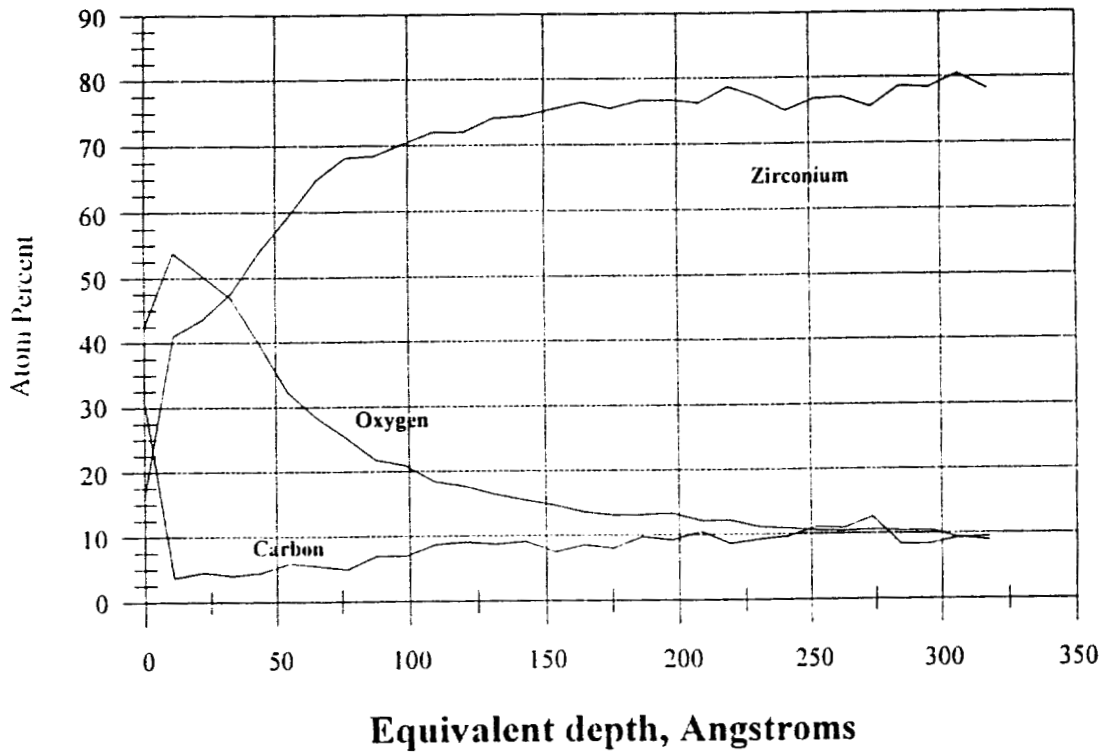

Figure 4-20. XPS Depth Profile for Zr-702 Air-Formed Film (uncorrected)

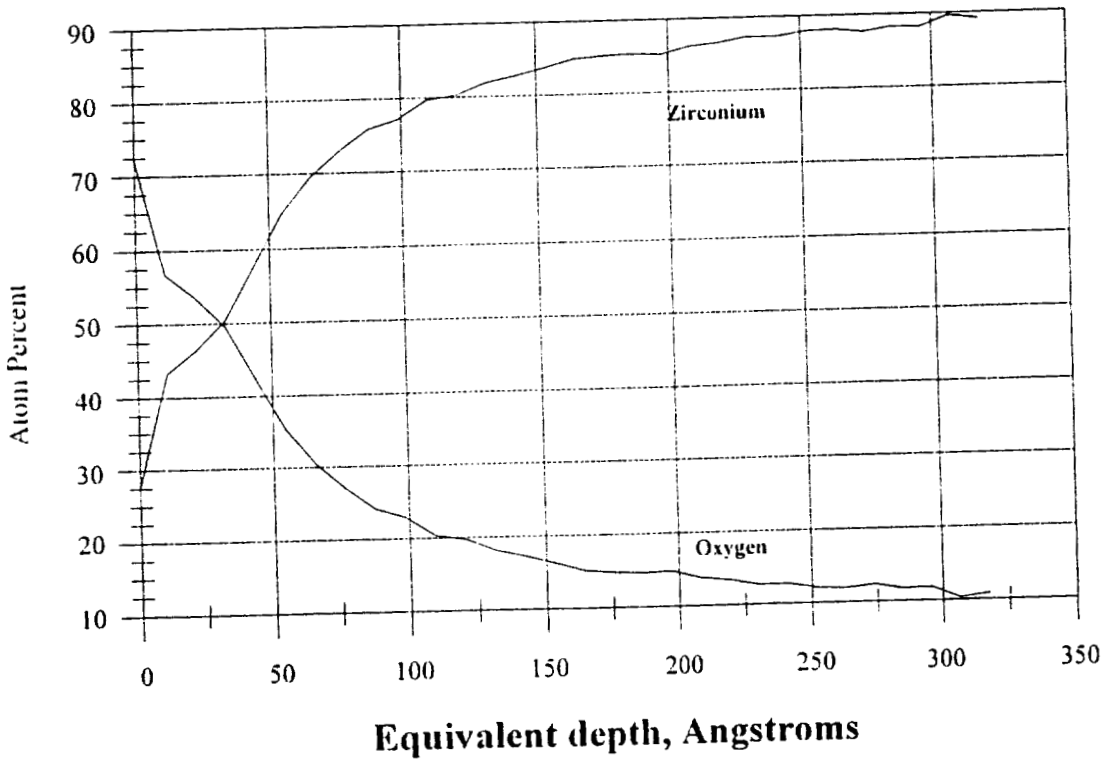

Figure 4-21. XPS Depth Profile for Zr-702 Air-Formed Film (renormalized)

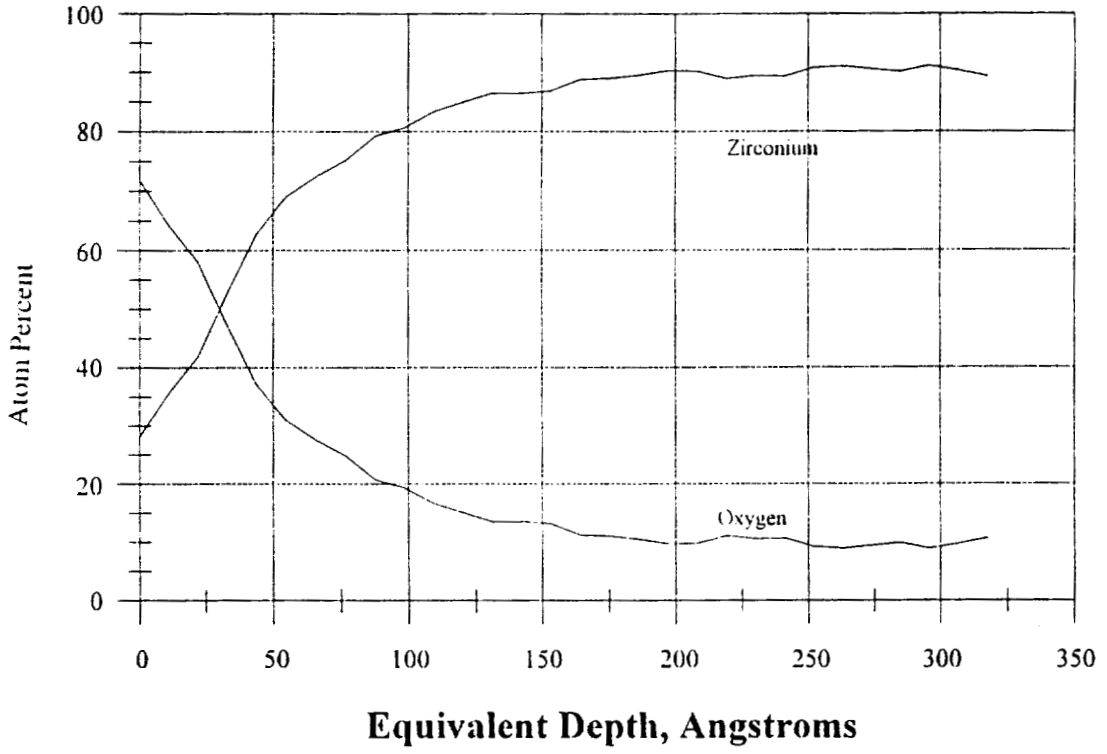

Figure 4-22. XPS Depth Profile for Zr-702 After Potentiodynamic Experiment in 1M Hydrochloric Acid at 0V

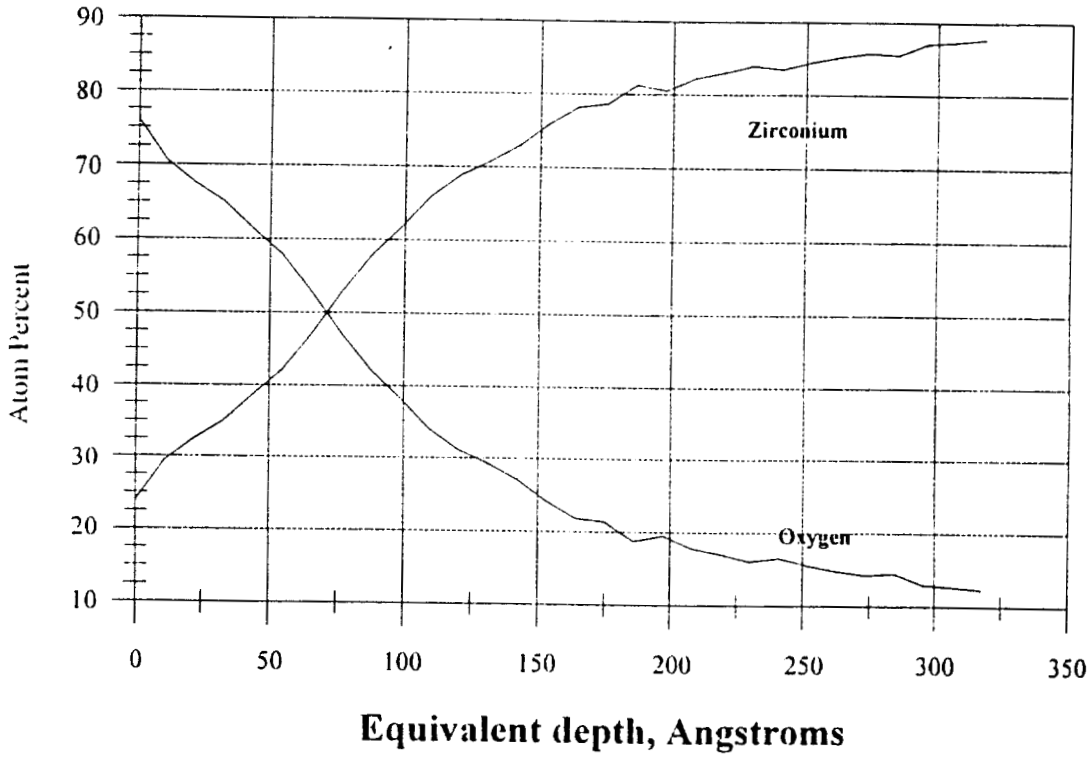

Figure 4-23. XPS Depth Profile for Zr-702 After Potentiodynamic Experiment in 1M Sulfuric Acid at 0V

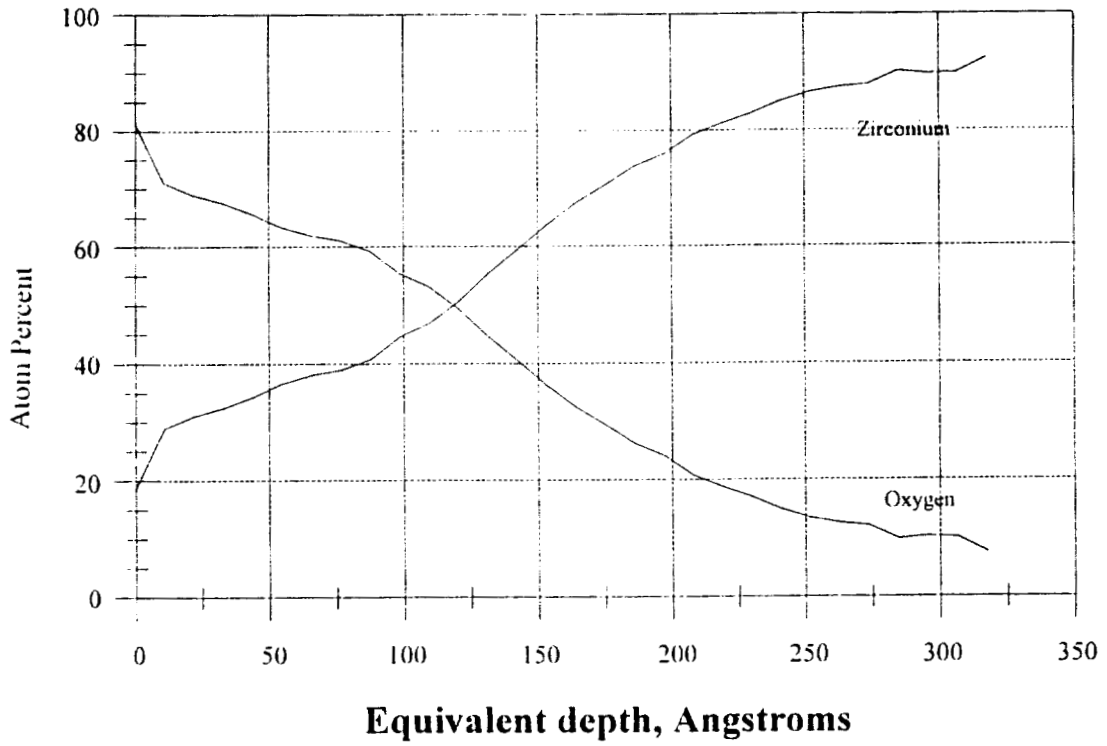

Figure 4-24. XPS Depth Profile for Zr-702 After Potentiodynamic Experiment in 1M Sulfuric Acid at 3V

4.5 EIS

4.5.1 Bode and Nyquist Plots

The Bode Plot for Zr-702 in aqueous sulfuric acid at 0V is shown in Figure 4-25. The |Z| vs frequency plot can be used to determine the characteristic resistances of the solution and the film, as shown in Figure 2-4. The high-frequency |Z| represents the solution resistance (R_a), and in this solution is very low; at the low frequencies, |Z| represents the sum of the solution and film resistances ($R_a + R_f$); in this case, the limit had not been reached at the lowest frequencies measured (0.005 Hz). The measured film resistance is several orders of magnitude greater than the solution resistance, a high film resistance indicating a low corrosion rate. Figure 4-26 is the Nyquist plot for the same sample; this figure shows the characteristic extension to the classic half circle, indicating that this reaction is diffusion controlled.

Figure 4-27 is the Bode plot for Zr-702 in hydrochloric acid. Again, we see that the solution resistance is quite low, and the film resistance very high. Figure 4-28 is the Nyquist plot for the same experiment; again, we see that the reaction is diffusion-controlled.

Figure 4-29 is the Bode plot for Zr-702 in aqueous-methanolic sulfuric. At frequencies above about 0.5 Hz, the behavior of this system is similar to that found in the aqueous sulfuric acid and hydrochloric acid experiments. Considerable noise exists in the low frequency data, however.

Figure 4-30 is the Bode plot for Zr-702 in aqueous sulfuric acid at 3V. At this voltage, the system can reach a limit at the lower frequencies, and a film resistance can be estimated.

In order to determine the effect of alloying, EIS curves were generated for Zr-704

in aqueous sulfuric acid, at 0V and 3V. Figure 4-31 shows the Bode plot for zero volts; the results are very similar to those found in Zr-702, with a very low solution resistance, and a high film resistance. The Nyquist plot, Figure 4-32, shows that the film grows under diffusion control. Figure 4-33 is the Bode plot for Zr-704 in sulfuric acid at 3V.

The solution and film resistances calculated by the model for each experiment are listed in Table 4-3.

Table 4-3. Summary of EIS Model Results

Alloy	Solution	Potential	Rs (ohm)	Rf (ohm)
702	aqueous sulfuric	0V	0.95	384550
702	aqueous hydrochloric	0V	.92	239440
702	methanolic sulfuric	0V	1.6	211.6
702	aqueous sulfuric	3V	6.9	458232
704	aqueous sulfuric	0V	1.218	708410
704	aqueous sulfuric	3V	6.2	282110

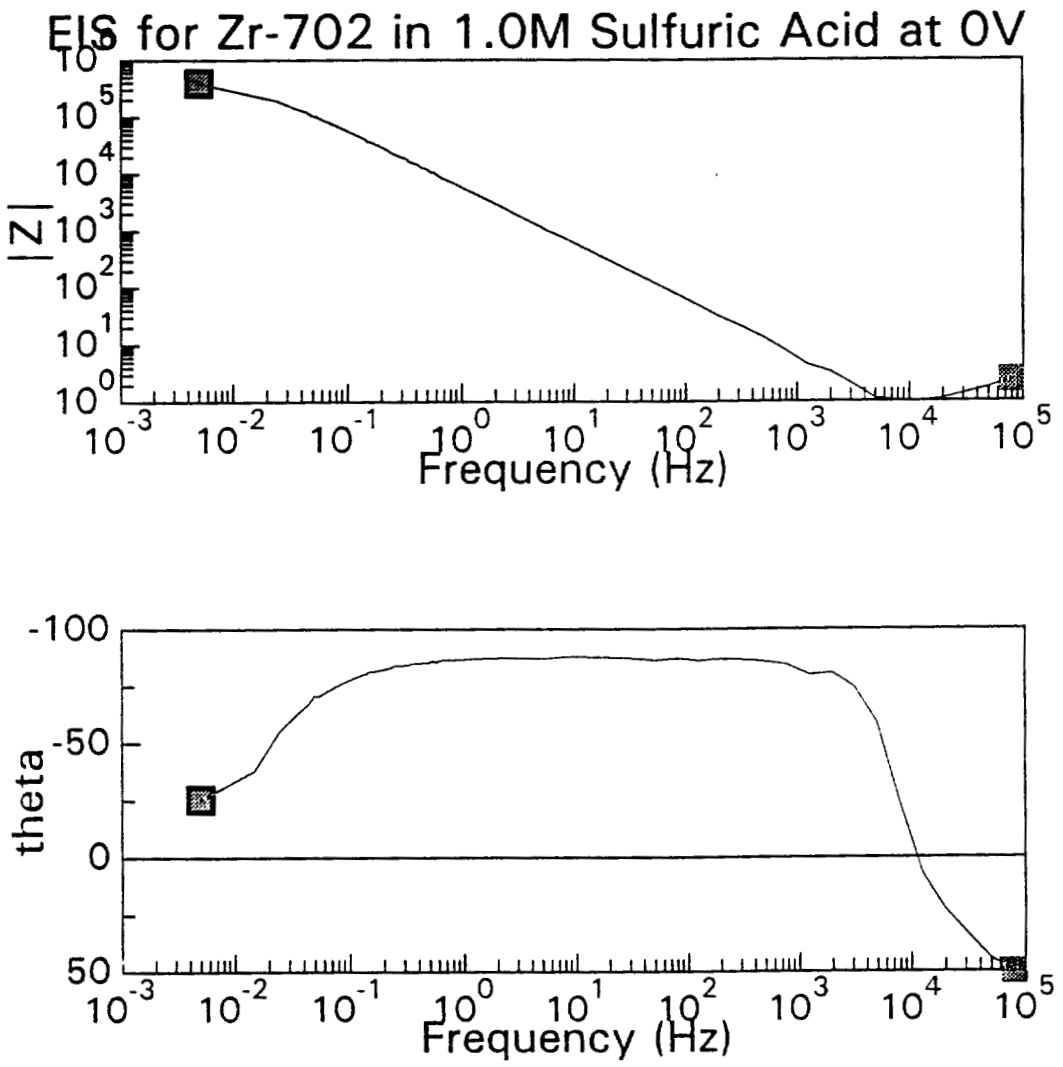

Figure 4-25. Bode Plot for Zr-702 in 1M Sulfuric Acid at 0V

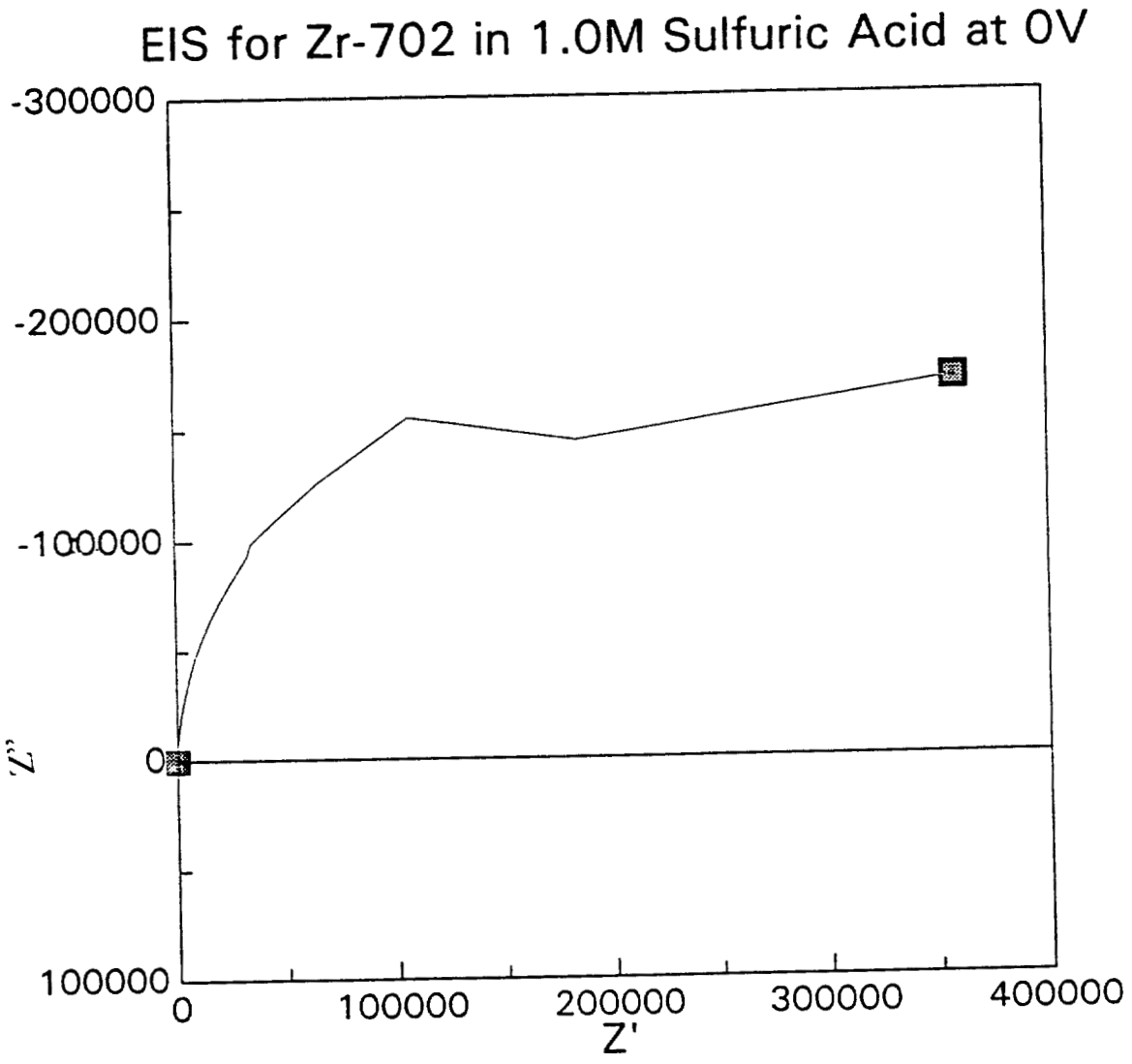

Figure 4-26. Nyquist Plot for Zr-702 in 1M Sulfuric Acid at 0V

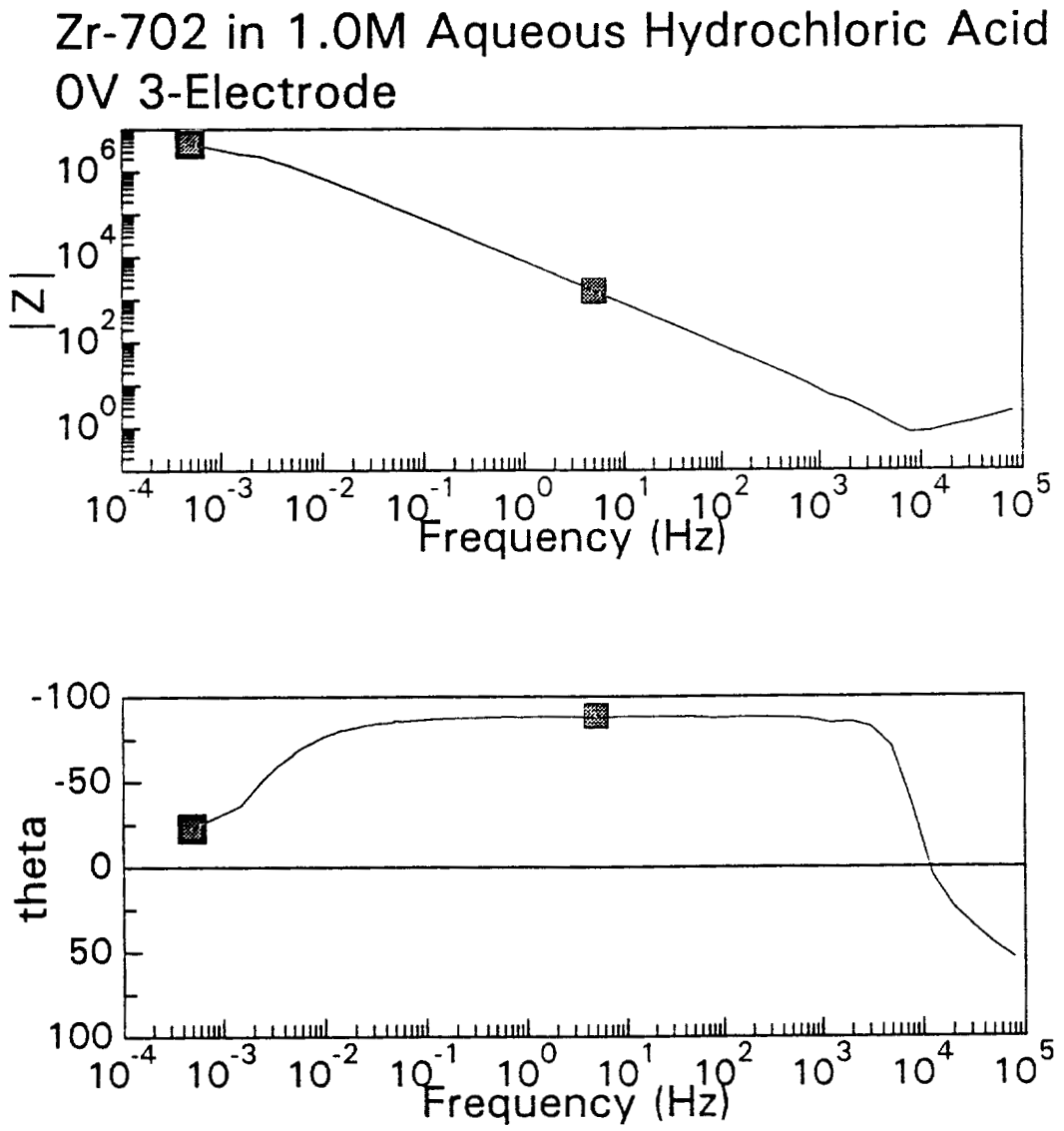

Figure 4-27. Bode Plot for Zr-702 in 1M Hydrochloric Acid at 0V

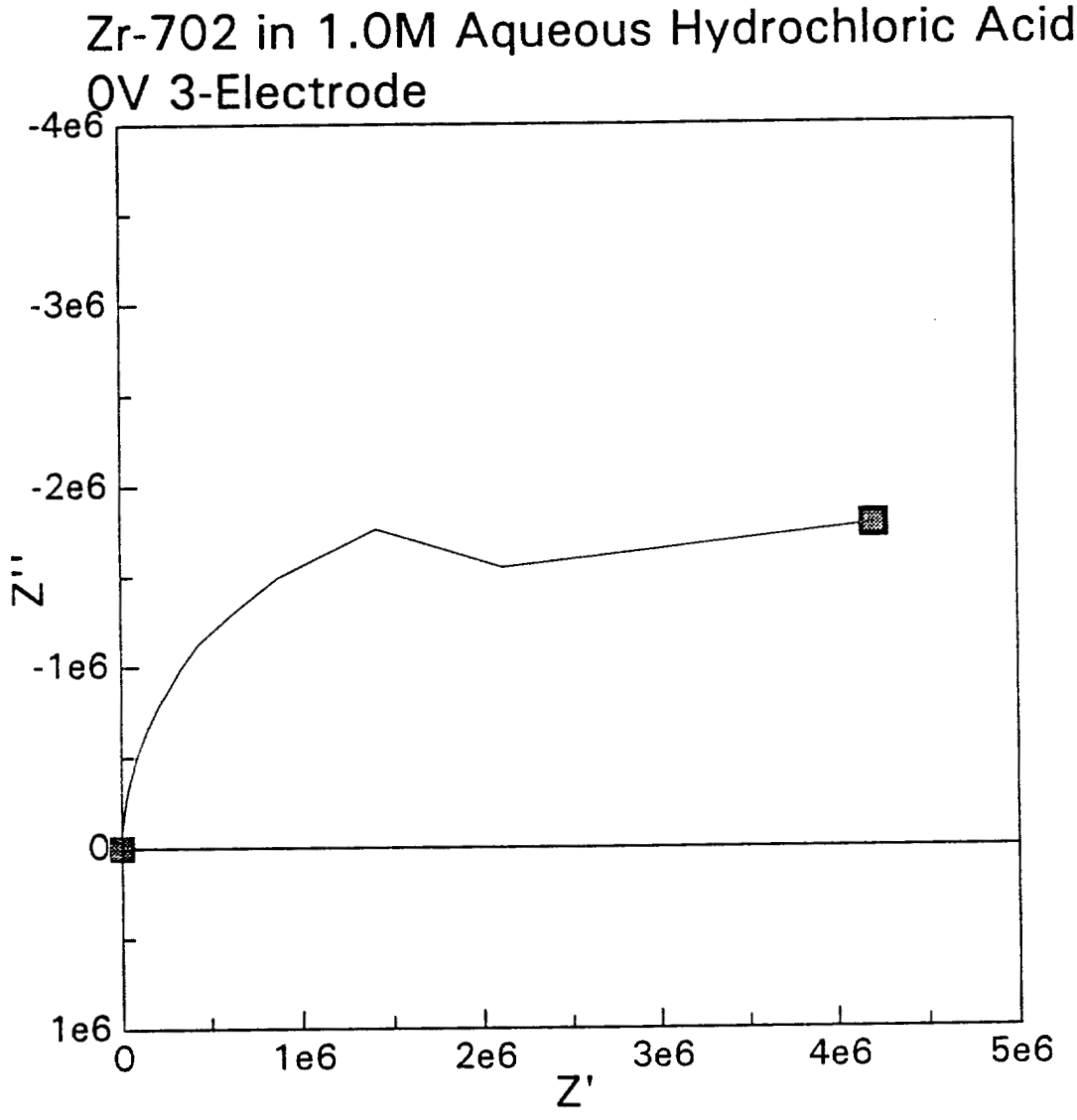

Figure 4-28. Nyquist Plot for Zr-702 in 1M Hydrochloric Acid at 0V

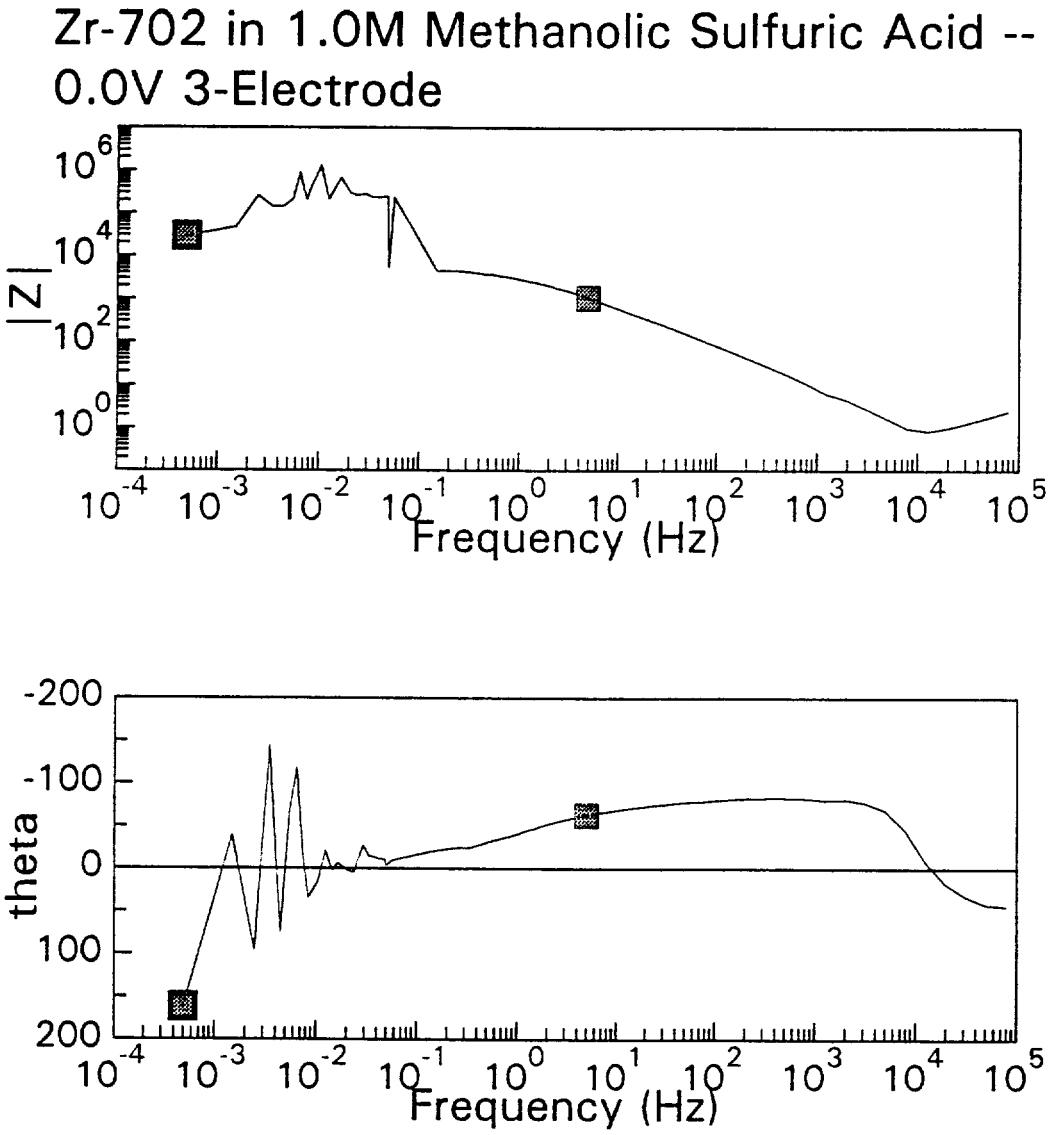

Figure 4-29. Bode Plot for Zr-702 in 1M Aqueous-Methanolic Sulfuric Acid at 0V

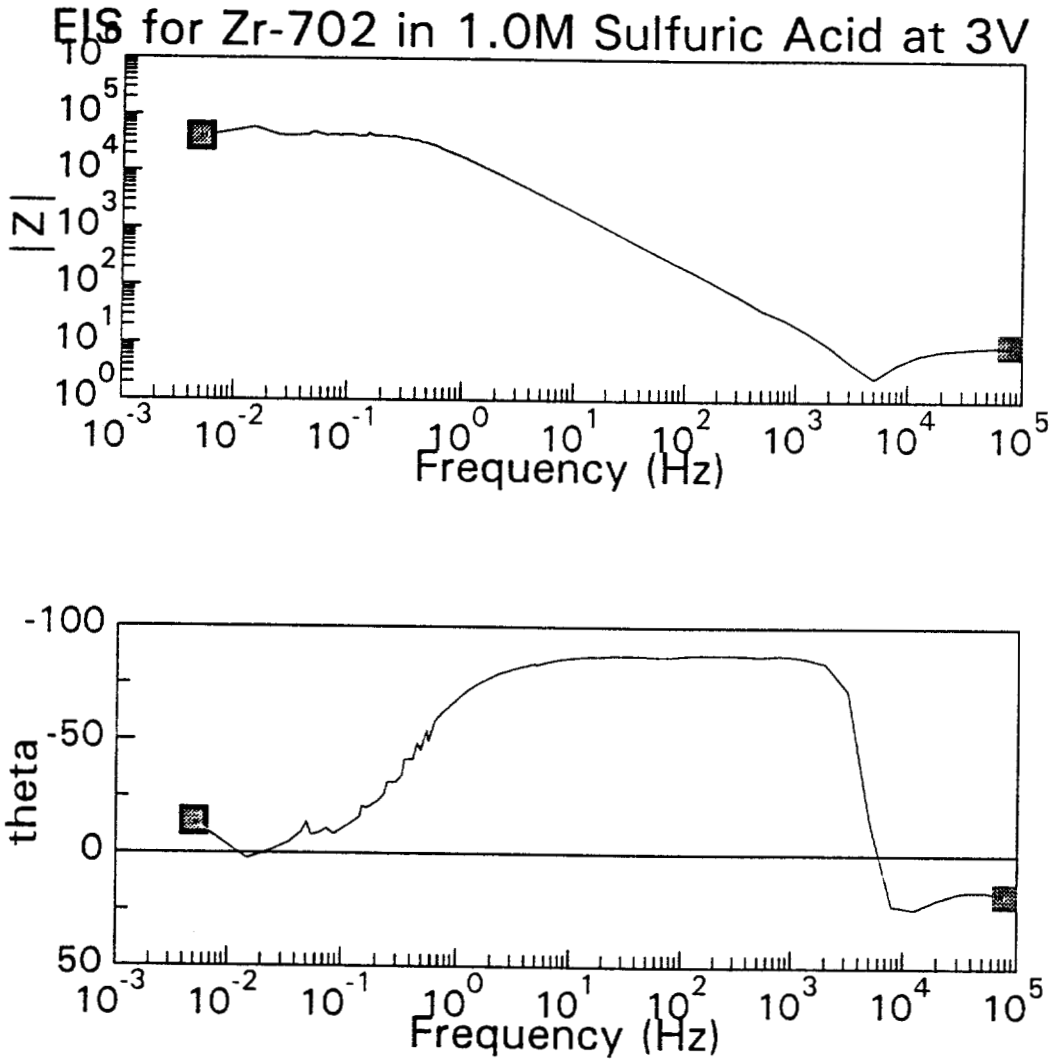

Figure 4-30. Bode Plot for Zr-702 in 1M Sulfuric Acid at 3V

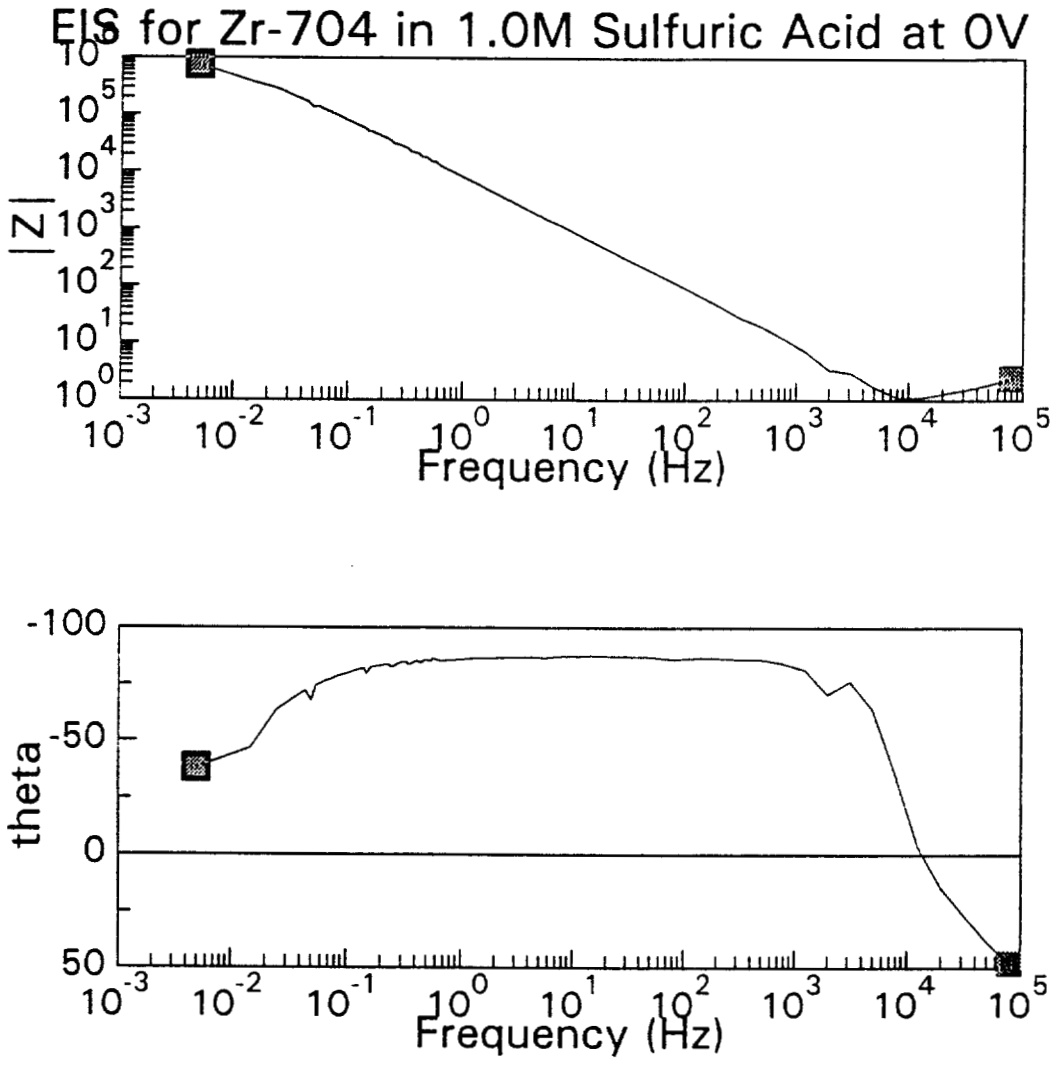

Figure 4-31. Bode Plot for Zr-704 in 1M Sulfuric Acid at 0V

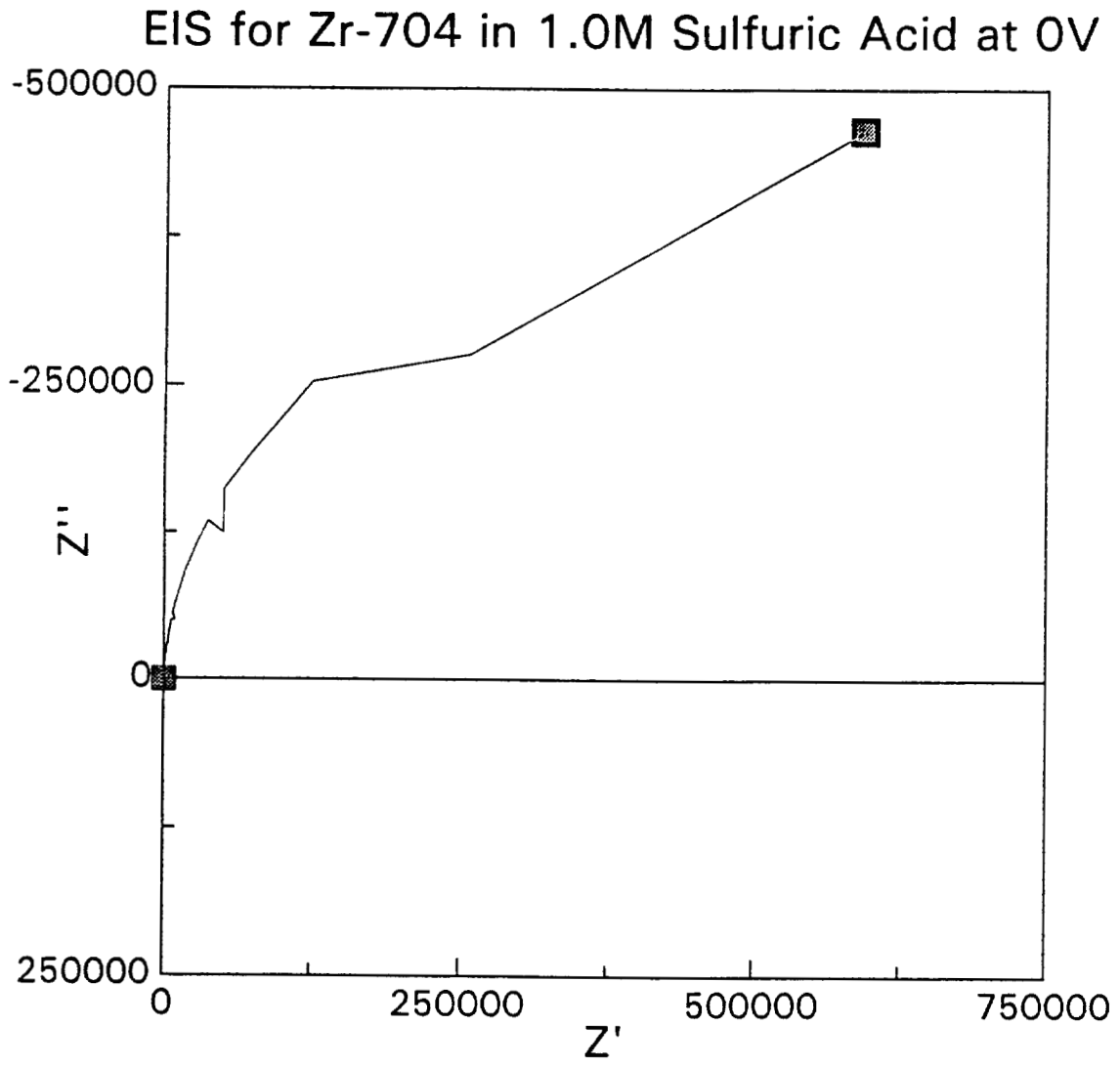

Figure 4-32. Nyquist Plot for Zr-704 in 1M Sulfuric Acid at 0V

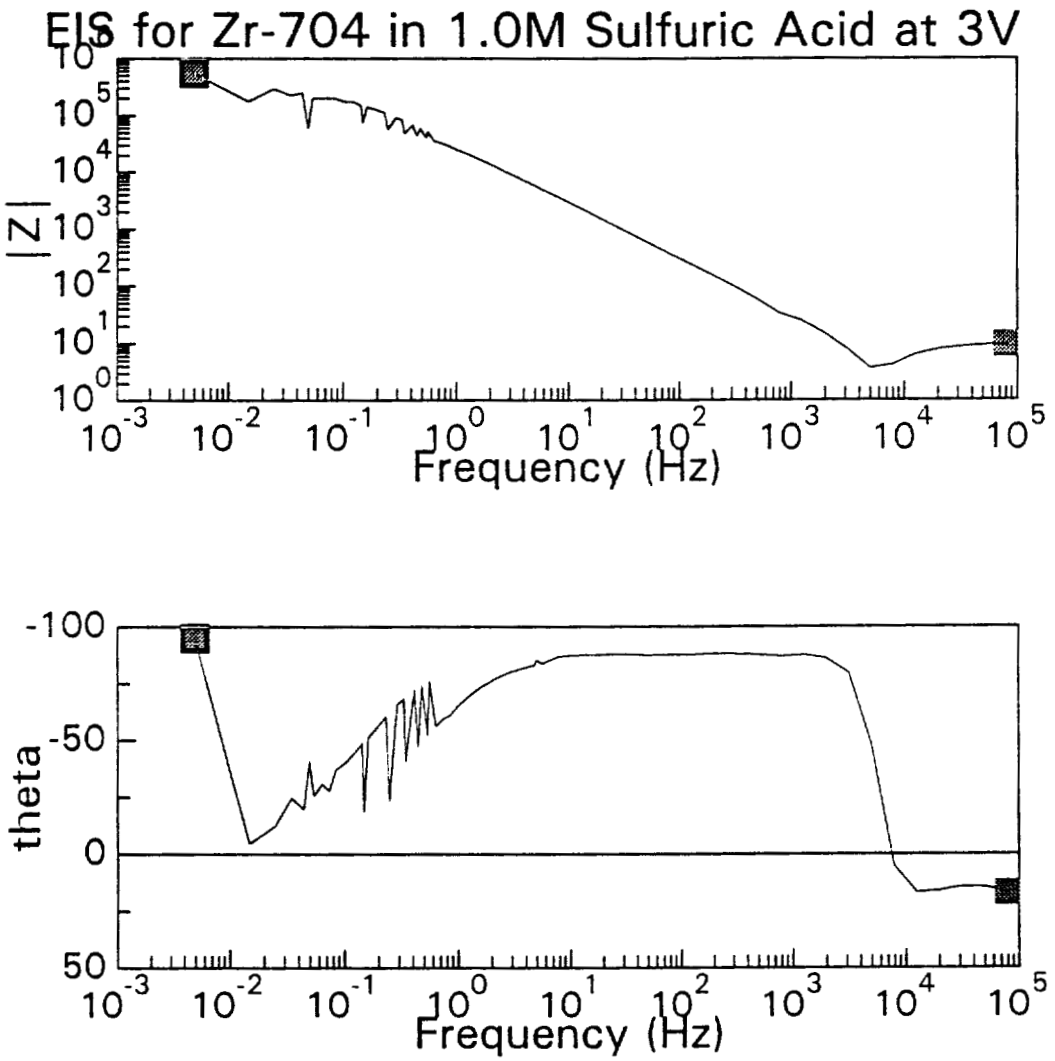

Figure 4-33. Bode Plot for Zr-704 in 1M Sulfuric Acid at 3V

4.5.2 Mott-Schottky Plots

Figure 4-34 is the Mott-Schottky plot for Zr-702 in 1M sulfuric acid at 3V. By calculating the slope, the value of the donor density for this system can be calculated. Table 4-4 lists the calculated donor densities.

Table 4-4. Mott-Schottky Plots

ALLOY	SOLUTION	POTENTIAL	DONOR DENSITY
Zr-702	aqueous sulfuric	1V	7.13×10^{19}
Zr-702	aqueous-methanolic sulfuric	0V	3.53×10^{19}
Zr-702	aqueous hydrochloric	0V	1.42×10^{19}
Zr-702	aqueous sulfuric	3V	1.70×10^{19}

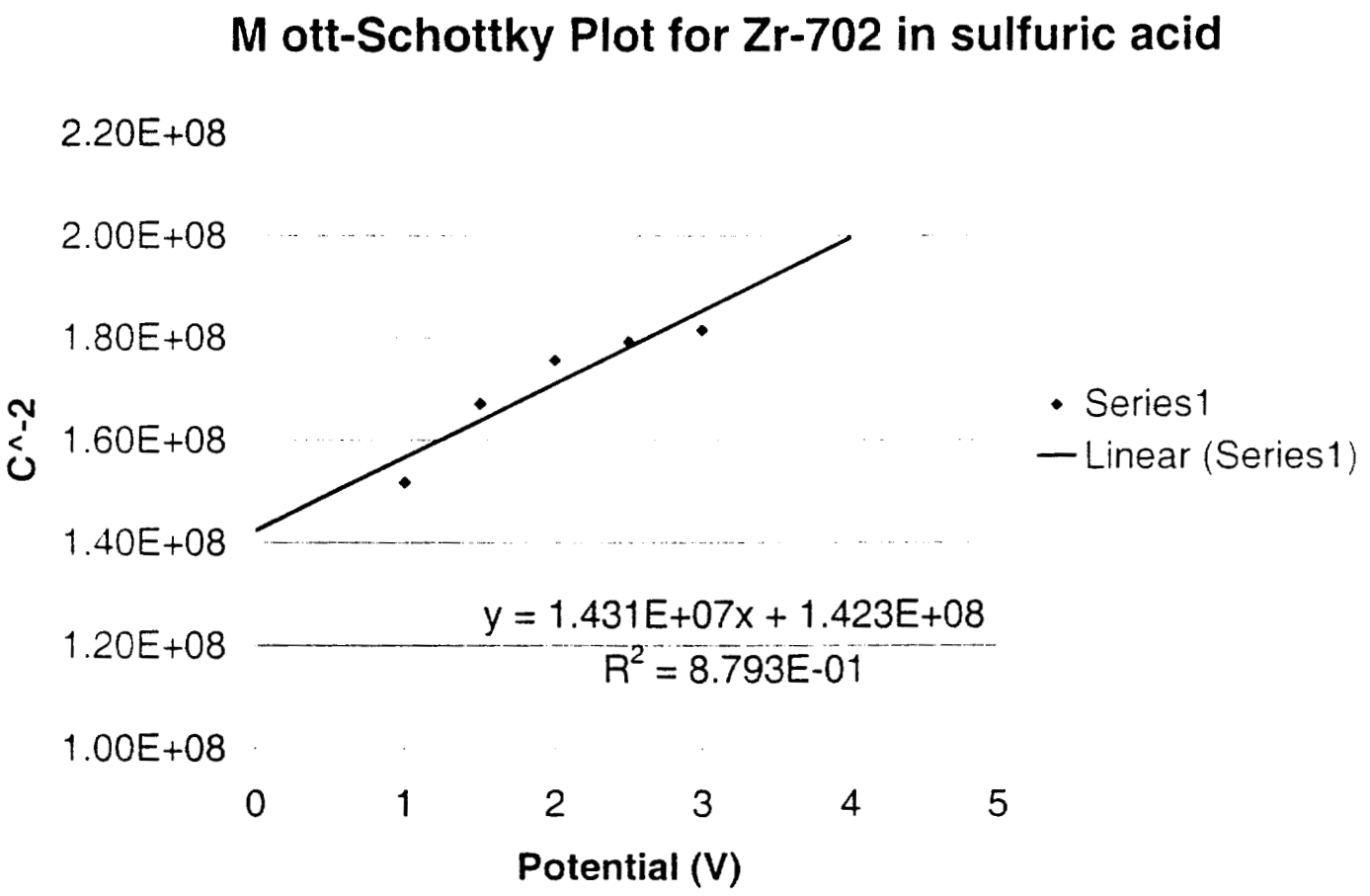

Figure 4-34. Mott-Schottky Plot for Zr-702 in 1M Sulfuric Acid at 3V

5.0 Discussion

5.1 Passivity

Zr-702 and Zr-704 show passive behavior in aqueous sulfuric acid, aqueous hydrochloric acid, and aqueous-methanolic sulfuric acid. The passive behavior in both sulfuric acid solutions is shown in their polarization curves, Figures 4-2 and 4-4. In hydrochloric acid, the polarization curves do not show this passive behavior; however, the potentiostatic tests at 0V (Figure 4-8) show that both alloys remain passive in 1.M hydrochloric acid at this potential. The current density for both alloys remains low, and decreases with time, characteristic of passive behavior.

XPS results show that the chemistry of the passive films formed on Zr-702 in sulfuric and hydrochloric acid are the same, containing only zirconium and oxygen. At the surface, the ratio of Zr:O is about 2:1, indicating that the film is made of ZrO_2. As the depth increases, the oxygen content decreases, down to about 10%. No uptake of electrolyte ions was found using EIS (Figure 4-18) The passive films formed in sulfuric acid are thicker than those formed in hydrochloric acid. The passive films formed on Zr-702 in sulfuric acid at 3V were considerably thicker than those formed at 0V, with significant oxygen diffusion into the metal. (Figure 4-24)

EIS experiments indicate that the passive film formation is a diffusion-controlled process, as shown in the Nyquist plots for Zr-702 in sulfuric and hydrochloric acid, respectively, at 0V (Figures 4-26 and 4-27). The deviation from the classic Nyquist semicircle shows the presence of the diffusion-controlled reaction.

5.2 Passivity Breakdown

The breakdown of the passive film on Zr-702 and Zr-704 has been demonstrated in two solutions: 1M hydrochloric acid and 1M aqueous-methanolic sulfuric acid. In hydrochloric acid, the breakdown results in localized corrosion, forming pits, as seen in

Figure 4-14. In aqueous-methanolic sulfuric acid, the low water content of the sample limits passivation, allowing the passive film to break down. At elevated potentials, this breakdown can lead to a smoothing of the surface, indicating a uniform breakdown of the film. [3]

5.3 Electronic Behavior of Passive Films

EIS testing allowed the modeling of the solution/film/metal system, as shown in Figure 2-4. The highest film resistances as listed in Table 4-2, were found for the 1M sulfuric acid experiments at 0V. Lower resistances in the hydrochloric acid experiments at 0V tend to indicate that these films may be less protective. In the aqueous-methanolic sulfuric acid experiments at 0V, the film resistance was three orders of magnitude lower than that for the aqueous solutions, indicating that the limited water content made the solution much more aggressive towards Zr-702.

Mott-Schottky curves (C^{-2} vs V) were used to determine the doping density, and thus the defect concentration, in the films formed on Zr-702. The donor density was lowest for the hydrochloric acid solution; this may have been due to the thinness of the film; because there a negligible difference in the film thickness between the films formed in air and hydrochloric acid, as measured by XPS, the air-formed film dominates the semiconductor behavior of the film, and shows few defects. In thicker films formed in sulfuric acid, the donor density was much higher, indicating that rapid film growth could lead to higher defect concentrations. For the very thick films formed in sulfuric acid at 3V, the donor density was lower. The polarization curve for Zr-702 in sulfuric acid (Figure 4-1) shows a small increase in the passive current at above 2 V. It is possible that this increase is due to a change in film characteristics, such as crystallinity. The donor

density in this film is much smaller than that for the film formed at 1V, indicating that the film formed at higher potentials has fewer defects, which could explain the higher current density.

6.0 Summary

Zirconium shows passive behavior in sulfuric acid. No transpassive behavior was found in aqueous sulfuric acid; however, tranpassive behavior can be induced by reducing the water content of the solution by adding methanol.

Zirconium shows no noticeable passive region in the anodic polarization curve in aqueous hydrochloric acid, and at higher potentials shows localized corrosion (pitting).

The alloying of zirconium with small amounts of tin, iron and chrome appears not to have a significant effect on the corrosion or oxidation behavior of zirconium. Slightly higher current densities occur in the alloy at elevated potentials.

There is no significant uptake of electrolyte ions into the passive film observed by XPS.

Passive oxide films formed on Zr-702 in hydrochloric acid at 0V show no thickness increase over air-formed films.

Passive oxide films formed on Zr-702 in sulfuric acid at 0V are significantly thicker than those for air-formed films.

EIS experiments demonstrated that the passive film formed on zirconium acts as a semiconductor, and can be modeled by a simple resistor and capacitor circuit.

The film resistances calculated by EIS are the highest in aqueous sulfuric acid, and the lowest in aqueous-methanolic sulfuric acid.

Donor densities calculated for the oxide film grown in each electrolyte were between 10^{19} and 10^{20} cm^{-3}; the highest doping concentration was measured for films formed in aqueous sulfuric acid, indicating that the thicker films have a higher incidence of defects.

7.0 Future Work

The most important part of the future work is increasing the number of *in situ* techniques. In situ techniques allow the investigation of the mechanisms at work only during the test. Ex situ techniques, such as XPS, become problematic, as films can change during the period of time between film growth and XPS measurement

7.1 Photo techniques

7.1.1 Reflectance

Reflectance can be used to measure film thickness as a function of time [2] during the film-growing experiments. Real-time comparison of current density versus thickness during potentiostatic tests would allow the development of a film-growth model.

7.1.2 Photoelectrochemical Impedance Spectroscopy (PEIS)

PEIS involves shining an ultraviolet light on the sample while performing EIS tests. I would like to perform some PEIS tests on zirconium, to determine if there is a difference in bandgap energy between the films formed in each electrolyte.

7.2 Water content

I would like to see how the concentration of water in the aqueous-methanolic electrolyte affects the properties of the film. These tests would involve potentiodynamic, potentiostatic, and EIS experiments.

7.3 Additional XPS studies

Although it is an *ex situ* measurement, XPS has proven valuable in this thesis. I would like to do several more XPS samples for each solution and each alloy.

7.4 Crystallographic studies

Using x-ray diffraction, determine if the crystallinity of the passive film changes as a function of potential after potentiostatic tests. This would probably also have to be done *ex situ* as well.

7.5 Atomic Force Microscopy (AFM)

AFM can be used to detect the local potential on a surface *in situ*, potentially identifying the sites where pits could initiate.

8.0 References

[1] Schemel, J.H., ASTM Manual on Zirconium and Hafnium, American Society of Testing and Materials, ASTM Special Technical Publication 639, 1977.

[2] Yau, T.-L., "Corrosion of Zirconium," The Corrosion Engineering Handbook, New York, Dekker, 1996, pp.195-252.

[3] Ziomek-Moroz, M., VanWinkle, J., and Yau, T.-L., "Surface Finish Improvement of Zirconium in Organic Solutions," Proceedings of the 30th IMS Conference, 1997, pp. 35-39.

[4] Bailar, J.C., et al, eds, Comprehensive Organic Chemistry -- Volume 3, Pergamon Press, New York, 1973.

[5] Jones, D.A.,Principles and Prevention of Corrosion, Prentice-Hall, Inc., 1996.

[6] Li, Y., Shimada, H., Sakiara, M., Shigyo, K., Takahashi, H., and Seo, M., "Formation and Breakdown of Anodic Oxide films on Aluminum in Boric Acid/Borate Solutions," Journal of the Electrochemical Society, Vol. 144, No. 3, March 1997, pp. 866-876.

[7] Urquidi-Macdonald, M., and Macdonald, D.D., "Solute-Vacancy Interaction Model and the Effect of Minor Alloying elements of the Initiation of Pitting Corrosion," Journal of the Electrochemical Society, Vol. 132, No. 3, March 1985, pp.555-558.

[8] Schmuki, P and Virtanen, P., "Experimental Modeling of Passivity," Interface. Vol 6. No. 2, 1997, pp. 38-42.

[9] Sato, N., "An Overview on the Passivity of Metals," Corrosion Science, Vol. 30, 1990, pp. 1-19.

[10] Salot, R., Lefebre-Joud, F., and Baroux, B., "Electrochemical Behavior of Thin Anodic Oxide Films on Zircaloy-4 Role of the Mobile Defects," Journal of the Electrochemical Society Vol. 143, No. 12, December 1996, pp 3902-3909.

[11] Leach, J.S.L. and Pearson, B.R., "Crystallization in Anodic Oxide Films," Corrosion Science, Vol. 28, No. 1, 1988, pp 43-56.

[12] Fahey, J., Holmes, D., and Yau, T.-L., "Evaluation of Localized Corrosion of Zirconium in Acidic Chloride Solutions," Corrosion, Vol. 53, No. 1, January 1997, pp. 54-61.

[13] Balsamov, A.V., Lilin, S.A., and Rumyantsev, "Anodic Behavior of Zirconium in Aqueous Isopropanol Solutions of Sodium Chloride at High Potentials," Surface Engineering and Applied Electrochemistry, Vol. 2, 1993, pp 37-43.

[14] Khalil, N., Bowen, A., and Leach, J.S.L., "The Anodic Oxidation of Valve Metals – II. The Influence of the Anodizing Conditions on the Transport Processes During the Anodic Oxidation of Zirconium," Electrochimica Acta, Vol. 33 No. 12, 1988, pp. 1721-1727.

[15] Chao, C.Y., Lin, L.F., and Macdonald, D.D., "A Point Defect Model for Anodic Passive Films I. Film Growth Kinetics," Journal of the Electrochemical Society, Vol. 128, No. 6, June 1981, pp. 1187-1198.

[16] Macdonald, D.D., and Urquidi-Macdonald, U., "Theory of Steady-State Passive Films," Journal of the Electrochemical Society, Vol. 137, No. 8, August 1990, pp. 2395-2403.

[17] Wilhelm, S.M., and Hackerman, N., "Photoelectrochemical Characterization of the Passive Films on Iron and Nickel," Journal of the Electrochemical Society, Vol. 128. No. 8, August 1981, pp. 1668-1674.

[18] Urquidi-macdonald, M., and Macdonald, D.D., "Theoretical Analysis of the Effects of Alloying Elements on Distribution Functions of Passivity Breakdown," Journal of the Electrochemical Society, vol 136., No.4., April 1989, pp. 41-46.

[19] Azumi, K., Ohtsuka, and Sato, N., "Mott-Schottky Plot of the Passive Film Formed on Iron in Neutral Borate and Phosphate Solutions," Journal of the Electrochemical Society, Vol. 134, No. 6, June 1987, pp. 1352-1357.

[20]Sato, N., "An Overview on the Passivity of Metals," Corrosion Science, Vol. 30, 1990, pp 1-19.

[21] Castro, E.B., Vilche, J.R., and Oliveira, C.L.F., "A Comparative EIS Study of Passive Layers Formed on Iron and Iron-Chromium Alloys," Materials Science Forum, Vols 192-194, 1995, pp. 611-622.

[22] Kloppers, M.J., Bellucci, F., and Latanision, R.M., "Electronic Properties and Defect Structure of Fe and Fe-Cr Passive Films," Corrosion, Vol. 48, No. 3, March 1992, pp.229-238.

[23] Macdonald, D.D., Sikora, E., and Sikora, J, "A New Method for Estimating the Diffusivities of Vacancies in Passive Films,"Electrochimica Acta Vol. 41, no. 6, April 1996, pp. 783-789.

[24] Azumi, K., Ohtsuka, T., and Sato, N., "Mott-Schottky Plot of the Passive Film Formed on Iron in Neutral Borate and Phosphate Solutions," Journal of the Electrochemical Society, Vol. 134, No. 6, June 1987, pp.1352-1357.

[25] van de Krol, R. Goosens, A., and Schoonman, J., "Mott-Schottky Analysis of Nanometer-Scale Thin-Film Anatase TiO_2," Journal of the Electrochemical Society, Vol. 144, No.5, May 1997, pp. 1723-1727.

[26] Nogami, G., "Theory of Capacitance-Voltage Characteristics of Semiconductor Electrodes with Interface States," Journal of the Electrochemical Society, Vol. 133, No.3, March 1986, pp. 525-531.

[27] Schoonman, J., Vols, K., and Blasse, G., "Donor Densities in TiO_2 Photoelectrodes," Journal of the Electrochemical Society, Vol 128, No. 5, May 1981, pp. 1154-1157.

[28] Kennedy, John H., and Frese, K.W., "Flatband Potentials and Donor Densities of Polycrystalline alpha-Fe2O3 Determined from Mott-Schottky Plots," Journal of the Electrochemical Society Vol. 125, NO. 5, May 1978, pp. 723-726.

[29] Su, Wei, "Study of Passivation Behavior for Titanium Aluminides ", Oregon Graduate Institute of Science and Technology Ph.D. Thesis.

[30] Shigolev, P.V., Electrolytic and Chemical Polishing of Metals, 2nd edition, Tel Aviv, Freund, 1974.

[31] Morris, P.E. and Scarberry, R.C., "Predicting Corrosion Rates with the Potentiostat," Corrosion, Vol. 28 No. 12, December 1972, pp. 444-452.

[32] Urquidi-Macdonald, M., and Macdonald, D.D., "Theoretical analysis of the Effects of Alloying Elements on Distribution Functions of Passivity Breakdown," Journal of the Electrochemical Society, Vol. 136, No. 4., April 1989, pp. 961-967.

[33] da Fonseca, C., and da Cunha Belo, M., "A Characterization of Titanium Passivation Films by In-Situ AC Impedance Measurements and XPS Analysis," Materials Science Forum, Vols. 192-194, 1995, pp. 177-184.

[34] Nogami, G., "Some Aspects of Large Frequency Dispersion of Mott-Schottky Plots in TiO_2 Electrodes," Journal of the Electrochemical Society, Vol. 132, No.1, January 1985, pp. 76-81.

[35] Su, Wei, Ziomek-Moroz, M., and Covino, B.S., "Study of Passive Films on alpha-2 and gamma Titanium Aluminides," Microstructural Science Vol. 25 (USA), pp. 21-28, 1998

[36] Masnfeld, F., Kendig, M.W. and Tsai, S., "Recording and Analysis of AC Impedance Data for Corrosion Studies II. Experimental Approach and Results," Corrosion, Vol. 38, No. 11, November 1982, pp 570-580.

[37] Macdonald, D.D., "Some Advantages and Pitfalls of Electrochemical Impedance Spectroscopy," Corrosion, Vol. 46, No.3, March 1990.

[38] Mansfeld, F., "Recording and Analysis of AC Impedance Data for Corrosion Studies I. Background and Methods of Analysis," Corrosion, Vol. 36, No. 5, May 1981, pp. 301-307.

[39] Characteristic X-Ray Emission Energies (Wall Chart), Princeton Gamma Tech, Princeton, NJ.

[40] Leitner, K., Schultze, J.W., and Stimming, U., "Photoelectrochemical Investigations of Passive Films on Titanium Electrodes," Journal of the Electrochemical Society, Vol. 133, No. 8., August 1986, pp.1561-1568.

[41] Goosens, A., Vazquez, M., and MacDonald, D.D., "The Nature of Electronic States in Anodic Zirconium Oxide Films Part 2: Photoelectrochemical Characterization," Electrochimica Acta, Vol. 41, No. 1. 1996.

[42] Burstein, G.T., and Whillock, G.O.H., "The Dissolution and Repassivation of New Titanium Surfaces in Alkaline Methanolic Solution Part I. The Phenomena," Journal of the Electrochemical Society, Vol. 136, No. 5, May 1989, pp. 1313-1319.

[43] Burstein, G.T., and Whillock, G.O.H., "The Dissolution and Repassivation of New Titanium Surfaces in Alkaline Methanolic Solution Part II.The Kinetics," Journal of the Electrochemical Society, Vol. 136, No. 5, May 1989, pp. 1320-1327.

[44] Bertagna, V., Plougonven, C, Rouelle, F, and Chemla, M., "p- and n-Type Silicon Electrochemical Properties in Dilute Hydrofluoric Acid Solutions," Journal of the Electrochemical Society, Vol. 143, No. 11, November 1996, pp. 3532-3538.

[45] DiPaola, A., Shukla, D., and Stimming, U., "Photoelectrochemical Study of Passive Films on Stainless Steel in Neutral Solutions," Electrochimica Acta, Vol. 36, No. 2, 1991, pp. 345-351.

[46] Macdonald, D.D. Sikora, E., Balmas, M.W., and Alkire, R.C., "The Photo-Inhibition of Localized Corrosion on Stainless Steel in Neutral Chloride Solutions," Corrosion Science, Vol. 38, No.1, 1996, pp. 97-103.

[47] Breslin, C.B., Macdonald, D.D., Sidora, E., and Sikora, J., "Photo-Inhibition of Pitting Corrosion on Types 304 and 316 Stainless Steels in Chloride-Containing Solutions," Electrochimica Acta, Vol. 42, No. 1, 1997, pp. 137-144.

[48] Breslin, C.B., Macdonald, D.D., Sidora, E., and Sikora, J.,"Influence of UV Light on the Passive Behavior of SS316–Effect of Prior Illumination," Electrochimica Acta, Vol. 42, No. 1, 1997, pp. 127-136.

[49] Gad Allah, A.G., and Mazhar, A.A., "Impedance Studies on the Anodic Passivity of Titanium in Aqueous Media of Different pH," Corrosion, Vol. 45, No. 5, 1989, pp. 381-386.

[50] Delnick, F.M., and Hackerman, N., "Passive Iron: A Semiconductor Model for the Oxide Film," Journal of the Electrochemical Society, Vol. 126, No. 5, May 1979, pp 732-741.

[51] Hakiki, N.E., Boudin, S., Rondot, B., and da Cunha Belo, M., "The Electronic Structure of Passive Films Formed on Stainless Steels," Corrosion Science, vol. 37, No. 11, 1995, pp. 1809-1822.

[52] Macdonald, D.D., "On the formation of Voids in Anodic Oxide Films on Aluminum," Journal of the Electrochemical Society, Vol. 140, No. 3, March 1993, pp. L27-L30.

[53] Macdonald, D.D., Ben-Haim, M., and Pallix, J., "Segregation of Alloying Elements into Passive Films," Journal of the Electrochemical Society, Vol. 136, No. 11, November 1989, pp. 3269-3273.

[54] Urquidi-Macdonald, M., and Macdonald, D.D., "Theoretical Distribution Functions for the Breakdown of Passive Films," Journal of the Electrochemical Society, Vol. 134, No. 1, January 1987, pp. 41-46.

[55] Urquidi, M., and Macdonald, D.D., "Solute-Vacancy Interaction Model and the Effect of Minor Alloying Elements on the Initiation of Pitting Corrosion," Journal of the Electrochemical Society, Vol. 132, No. 3, March 1985, pp.555-558.

[56] Fredlein, R.A., and Bard, A.J., "Semiconductor Electrodes XXI. The Characterization and Behavior of n-Type Fe_2O_3 Electrodes in Acetonitrile Solutions," Journal of the Electrochemical Society, Vol. 126, No. 11, November 1979, pp. 1892-1898.

[57] Olszowka, S.A., Manning, M.A. and Barkatt, A., "Copper Dissolution and Hydrogen Peroxide Formation in Aqueous Media," Corrosion, Vol. 48, No. 5, May 1992, pp. 411-418.

[58] Manning, P.E., "The Effect of Scan Rate on Pitting Potentials of High Performance Alloys in Acidic Chloride Solution," Corrosion/80: The International Corrosion Forum Devoted Exclusively to the Protection and Performance of Materials, March 1980, pp. 73/1-73/14.

[59] Morris, P.E. and Scarberry, R.C., "Anodic Polarization Measurements of Active-Passive Nickel Alloys by Rapid-Scan Potentiostatic Techniques," Corrosion, Vol. 26, No. 7, July 1970, pp169-179.

[60] Stroecker, J.G., and Siebert, O.W., "Practical Applications of the Corrosion Behavior Diagram; A Critical Evaluation," Corrosion/80: The International Corrosion Forum Devoted Exclusively to the Protection and Performance of Materials. March 1980, pp. 76/1-76/17.

[61] Greene, N.D., "The Classical Potentiostat: Its Application to the Study of Passivity," Corrosion. Vol 15, 1959, pp 369-372.

[62] "Recommended Practice for Standard Reference Method for Making Potentiostatic and Potentiodynamic Anodic Polarization Measurements." Annual Book of ASTM Standards, Vol. 3.02, G5-94, 1998 pp. 54-64.

[63] Baker, B.C., and West, A.C., Electrochemical Impedance Spectroscopy Study of Nickel-iron Deposition I. Experimental Results," Journal of the Electrochemical Society, Vol. 144, No. 1, January 1997, pp.164-175.

[64] Schmuki, P., Virtanen, S., Davenport, A.J., and Vitus, C.M., "Transpassive Dissolution of Cr and Sputter-Deposited Cr Oxides Studied by In Situ X-Ray Near Edge Spectroscopy," Journal of the Electrochemical Society, Vol. 143, No. 12, December 1996, pp.3997-4005.

[65] Burke, L.D., Healy, J.F., and Murphy, O.J., "Corrosion of Oxide-Coated Titanium (DSA) Anodes in Organic Solvents (Especially Methanol)," Applied Electrochemistry, Vol. 13, 1983, pp. 459-468.

[66] Schmuki, P., Virtanen, S., Davenport, A.J., and Vitus, C.M., "Dissolution of Thin Iron Oxide Films Used as Models for Iron Passive Films Studied by In Situ X-Ray Near Edge Spectroscopy," Journal of the Electrochemical Society, Vol. 144, No. 1, January 1997, pp. 198-204.

Biographical Sketch

James VanWinkle was born July 12, 1964 in Hillsboro, Oregon. He received a B.S. in Physics from Oregon State University in 1987, an M.S. from OSU in 1989, and an MS in Environmental Sciences and Engineering from the Oregon Graduate Institute of Science & Technology in 1997. From 1989 to 1993, he worked at the Trojan Nuclear Power Plant in both the Nucelar Safety group, as well as the Individual Plant Examination group performing safety analyses. From 1995-1998, he was a member of the OGI student council, serving as president from 1996-1998.